NASA TECHNICAL NOTE

NASA TN D-4919

NASA TN D-4919

THE PATH OF A JET DIRECTED AT LARGE ANGLES TO A SUBSONIC FREE STREAM

by Richard J. Margason

Langley Research Center
Langley Station, Hampton, Va.

NATIONAL AERONAUTICS AND SPACE ADMINISTRATION • WASHINGTON, D. C. • NOVEMBER 1968

NASA TN D-4919

THE PATH OF A JET DIRECTED AT LARGE ANGLES TO A SUBSONIC FREE STREAM

By Richard J. Margason

Langley Research Center
Langley Station, Hampton, Va.

NATIONAL AERONAUTICS AND SPACE ADMINISTRATION

For sale by the Clearinghouse for Federal Scientific and Technical Information
Springfield, Virginia 22151 – CFSTI price $3.00

THE PATH OF A JET DIRECTED AT LARGE ANGLES TO A SUBSONIC FREE STREAM

By Richard J. Margason
Langley Research Center

SUMMARY

An investigation was made in the Langley 300-MPH 7- by 10-foot tunnel to determine the path and general shape of the wake from a single jet exiting at large angles to the free stream through a range of effective velocity ratios (square root of the ratio of the free-stream dynamic pressure to the jet dynamic pressure). The jet-exit deflection angles ranged, in 30° increments, from 30° to 180° from the free stream. Photographs taken of the wake, which was a mixture of compressed air and water vapor, showed that the jet paths were essentially the same when the jet was exiting upward or downward as well as when the jet was located adjacent to a large surface or located away from adjacent surfaces. The primary variables determining the jet path are the deflection angle of the jet exit and the effective velocity ratio. The results were compared with equations for the jet path from other investigations, and the best empirical fit to these data was determined.

INTRODUCTION

Many V/STOL airplanes have been proposed which use jet engines for lift and thrust. Wind-tunnel investigations (refs. 1 and 2) have shown that interference between the jets and the free stream causes significant changes in the aerodynamic characteristics of the body, wing, and tail of some configurations. A primary factor determining the magnitude and distribution of this interference has been attributed (ref. 2) to the rolling up of the wake into a vortex pair downstream from the jet exit. An early analytic treatment of the rolling up of the jet is presented in reference 3.

The position of this vorticity is important in calculating the interference effects. However, accounting for the detailed changes in shape is exceedingly difficult. As a first step toward understanding these interference effects, the present paper is limited to a study of the mean path of the jet wake. Various aspects of this path have been studied when the jet is directed at large angles to a subsonic free stream. Most of the previous investigations considered either the jet directed perpendicular to the free stream or directed through only a limited range of angles. The results of the current investigation

present data defining the path of a jet for a wide range of deflection angles. The empirical equation obtained from these data is then compared with other data as well as with several empirical and theoretical calculations. The purpose of the present paper is to unify the available data for describing the path of a jet and to provide a single equation which will describe the path of the jet wake for a wide range of deflection angles.

Much of the previous work has been mentioned in two reviews (refs. 4 and 5) recently published. From these reviews and a search of the literature, the results of eight investigations (refs. 6 to 12) have been selected for comparison with the results of the present investigation. References 6 and 7 consider several jet-exit deflection angles in addition to the jet exit perpendicular to the free stream. Two of these investigations (ref. 6) present empirical equations for the path of a jet, and the third investigation (ref. 7) presents an analytic equation. The other investigations (refs. 8 to 12) consider only the jet perpendicular to the free stream. Two of the investigations (refs. 10 and 11) present empirical equations for the path of a jet. The investigation of reference 9 presented a graphical relation among dimensionless parameters which describes the position of the jet wake in space for the data obtained. The last of these investigations (ref. 12) refined the jet analysis procedure of Kirkpatrick (ref. 13) to develop a semiempirical model of the wake. Since comparisons in reference 12 of results from the semiempirical model with experimental data show that further work on the model will be required to obtain good agreement, only experimental results from this reference will be used in the present paper.

The current investigation used a water-injection flow-visualization technique to make the path of the wake from a jet visible. The jet was mounted in the Langley 300-MPH 7- by 10-foot tunnel at deflection angles which ranged, in increments of 30°, from 30° away from the free-stream direction to blowing directly into the free stream. These tests were performed with the effective velocity ratio (square root of free-stream dynamic pressure to jet dynamic pressure) varied from approximately 0.10 to as high as 0.85. Tests were also performed to determine the effect of a surface adjacent to the jet exit and the effect of the jet blowing upward or blowing downward. These results were compared with the results from references 3 to 9, and the best empirical fit to these data was determined.

SYMBOLS

The wind-axis system is used for presentation of all the data. As illustrated in figure 1, the data are presented with the observer looking in the positive Y-direction. As a result, the X-direction is positive to the left, and the Z-direction is positive downward. The units used for the physical quantities defined are given both in U.S. Customary

Units and in the International System of Units (SI). Factors relating these two systems are presented in reference 14. The symbols used are defined as follows:

a	constant used in equation (1)
b	constant used in equation (1)
C	constant of integration used in equation (3)
D	nozzle diameter, 1.00 inch (2.54 centimeters)
K	constant used in equation (1)
p	pressure, pounds/foot^2 (newtons/meter^2)
q	dynamic pressure, pounds/foot^2 (newtons/meter^2)
r	radial distance from the nozzle center line, inches (centimeters)
R	nozzle radius, inches (centimeters)
T	temperature, degrees Rankine (degrees Kelvin)
V	velocity, feet/second (meters/second)
V_e	effective velocity ratio, $\sqrt{\frac{\rho_\infty V_\infty^2}{\rho_j V_j^2}}$
x	horizontal distance measured positive upstream from center line of jet-exit plane, inches (centimeters)
z	vertical distance measured positive downward from center line at jet-exit plane, inches (centimeters)
δ_j	deflection angle of jet-exit center line measured positive with increasing angle away from direction of free stream, degrees
ρ	density, slugs/foot^3 (kilograms/meter^3)

Subscripts:

a	atmospheric
j	jet exit
t	total
z	vertical direction
∞	free stream

MODEL AND APPARATUS

The apparatus used in this investigation to introduce a jet into the center of the wind-tunnel test section is shown in figure 2(a). The 1-in-diameter (2.54 cm) convergent round nozzle was supported with a 1.9-in-diameter (4.83 cm) pipe which also supplied the compressed air. The apparatus was pivoted so that an arbitrary jet-efflux angle could be set without changing the location of the center of the nozzle-exit plane.

A portion of the investigation was conducted with the jet mounted flush with a ground board which was 4 ft (1.22 m) wide by 8 ft (2.44 m) long. This installation is sketched in figure 2(b) which shows that the center line of the nozzle was located 1.50 nozzle diameters downstream from the tapered leading edge of the ground plane. This location minimized the boundary-layer formation in front of the nozzle exit.

Some of the nozzle characteristics are presented in figures 3 and 4. The nozzle-exit pressure profiles at three jet dynamic pressures are presented in figure 3. These profiles are not uniform. The small difference between the maximum and minimum total pressure is approximately 6 percent of the nominal value at the exit at each pressure ratio. A second characteristic, the downstream pressure profiles of the jet exhausting into ambient air, is presented in figure 4. These data show the spread of the width of the jet and the decay of the dynamic pressure. The jet decay is presented in figure 5 as the variation of the peak dynamic pressure in each downstream pressure profile with downstream distance.

Photographs were taken of the air-water mixture emitted from the nozzle and are presented in figures 6 to 16. Most of the photographs (figs. 6, 7, and 12 to 16) were taken with the camera lens located 100 in. (2.45 m) from the center line of the nozzle, using 4- by 5-in. (10.16- by 12.70-cm) film. In these photographs, there are two sizes of grid in the background; the small grid near the nozzle exit represents 1 nozzle diameter and

the large grid away from the nozzle exit represents 2 nozzle diameters. A second group of photographs (figs. 8 to 11) were taken with a camera which used 70-mm film. To get the same field of vision, the camera had to be located about 145 in. (3.68 m) from the nozzle center line. In this second series of photographs, the small background grid represents multiples of 1.14 nozzle diameters. In both groups of photographs the correct scale is indicated. It can be seen that the scale in the photographs usually does not coincide with the grid in the background. The scale is alined with the nozzle exit. Since the nozzle is supported in the center of the wind tunnel by a 5-ft-long (1.52 m) pipe, the free stream deflects this pipe and changes the location of the nozzle exit relative to the grid on the wind-tunnel wall.

TEST TECHNIQUES

The jet wake was made visible by mixing a small amount of water with the compressed air approximately 6 ft (1.8 m) upstream of the nozzle-exit plane. Preliminary tests showed that this distance provided satisfactory mixing of the water and the air for visualization purposes. The amount of water was adjusted so that only the minimum required to make the wake visible was used.

The exit conditions for the nozzle were determined from detailed nozzle-exit pressure profiles (fig. 3) taken at several pressure levels and correlated with readings from static-pressure probes. The probes were located in the primary air supply line upstream from where the water vapor was introduced so that water vapor would not plug the lines from the static-pressure probes. During the investigation of the jet paths, the static pressure at the upstream end of the line was used to set the conditions at the nozzle exit. A particular effective velocity ratio was obtained by setting the desired exit dynamic pressure and then adjusting the tunnel dynamic pressure. Since the jet temperatures were nearly ambient, no temperature data were measured.

ACCURACY

The accuracy of the results presented depends primarily on two factors: the effective velocity ratio and the wake shape represented by the photographs.

The first factor, the effective velocity ratio, depends on the values of the free-stream dynamic pressure and the jet dynamic pressure. When the test section is clear, the free-stream dynamic pressure can be measured within ± 0.1 psf (± 5 N/m^2). For the free-stream dynamic pressures used, 10 to 170 psf (479 to 8140 N/m^2), this represents a range of error from 1.00 to 0.06 percent. For a jet of this size (fig. 2(a)) operating at

subsonic velocities, the blockage effect and the wind-tunnel wall interference are extremely small in the 7- by 10-foot (2.13- by 3.05-meter) test section. No corrections were made for these effects.

The other quantity, the value of the jet dynamic pressure, depends on the repeatability of the calibration described in the section "Test Techniques" and on the effect of the presence of the water in the jet. Checks made at intervals throughout the investigation demonstrated that the calibration could be repeated within 0.4 percent. The effect of the presence of the water could not be readily evaluated experimentally because probes placed in the nozzle exit would plug with water. In an effort to check this effect, a load cell was used to measure the thrust of the nozzle when a given value of pressure was obtained in the primary air supply line by using either air alone or air mixed with water. These results indicated a difference in the jet dynamic pressure due to the presence of the water ranging up to 7.2 psf (345 N/m^2). These effects represent a range of error from 0.6 to 5 percent in exit dynamic pressure. The nozzle-exit dynamic pressure and free-stream dynamic pressure combine to form the effective velocity ratio with an error ranging from 1 percent for values of effective velocity ratio near 0.1 to 3 percent for values near 0.8. The results obtained from the current investigation and from empirical equations of the jet show that errors in effective velocity ratio of this magnitude should not make significant changes in the path of the jet.

The second factor, the accuracy of the representation of the wake shape, is difficult to evaluate from the photographs. In reference 8, a detailed map of the pressure field through the wake was obtained and used to define the path of the wake as the locus of maximum pressures. This type of survey is outside the scope of the current investigation. Observation of the wake from several directions indicates the bulk of the mass flow is concentrated toward the upstream edge of the wake in the plane of the center line of the nozzle. This portion of the wake is used to define the path of jet wake in the present investigation. In the section "Results and Discussion," the paths obtained from an empirical equation based on the photographs are compared with results of eight other investigations (refs. 6 to 12). In most cases, the current results fit in the middle of the previous data. This indicates that the current procedure gives a result which is consistent with other methods.

RESULTS AND DISCUSSION

The results of the present investigation are presented in two sections: the jet wake at $\delta_j = 90^o$ and the jet wake at $\delta_j \neq 90^o$. These results are then compared with the results from eight previous investigations (refs. 6 to 12) in a third section.

Jet Wake at $\delta_j = 90^o$

The path of the jet exiting downward in the middle of the wind tunnel perpendicular to the free stream was photographed through a range of effective velocity ratios from 0.10 to 0.83. The results are presented in figure 6. An empirical equation was developed so that the jet paths could be compared with each other and with those from previous investigations. The form of this equation is similar to that used in references 2 and 11 to describe the locus of maximum pressures in the jet wake

$$\frac{x}{D} = K\left(\frac{z}{D}\right)^a V_e{}^b \tag{1}$$

The data presented in figure 6 were used to evaluate the constants K, a, and b; values of -1/4, 3, and 2, respectively, were obtained. The curves superimposed on the photographs show the correlation of this empirical equation to the jet path. In the range of effective velocity ratios from 0.4 to 0.6, the empirical curve indicates a little less penetration than shown by the photographs. In general, however, the path described by the empirical equation represents the center line of the jet wake.

The data in these photographs were obtained by using a jet of compressed air mixed with water vapor. Since the water vapor and the air have different densities, the resulting wake as shown in figure 6 might be different if the jet was pointed upward from what it was when the jet was pointed downward. The results presented in figure 7 show the wake shape when the jet is pointed upward for a range of effective velocity ratios from 0.21 to 0.85. The curves in the photographs were obtained from equation (1) and show that these results are essentially the same as those presented in figure 6. These data indicate that the results of blowing the jet upward and of blowing the jet downward are similar when the water vapor is used for flow visualization.

Since a given effective velocity ratio can be obtained from many combinations of free-stream dynamic pressure and jet dynamic pressure, the photographs presented in figures 8 to 10 were taken to determine the path of the jet wake at three values of effective velocity ratio (V_e = 0.10, 0.20, and 0.25) for different combinations of these pressures. The results in each of the three figures are similar to those in figure 6 as shown by the curves in the photographs which were obtained from equation (1). These results show that the jet path depends on the effective velocity ratio and that this ratio can be obtained with an arbitrary subsonic jet dynamic pressure and the appropriate free-stream dynamic pressure. This indicates that the effective velocity ratio is the predominant characteristic in determining the path of the jet wake at a given deflection angle.

All the preceding photographs were taken with the jet located in the center of the 7- by 10-foot (2.13- by 3.05-m) test section. The jet in this location is capable of inducing changes in the direction of the free stream above the plane of the jet exit as well as in the

vicinity of the jet wake. This raises the question of whether the location has a significant effect on the path of the jet wake. Several previous investigations (refs. 6, 8, 9, 10, and 12) have based their results on the wake path of a jet located in or near a wall of a wind tunnel. In this situation, there is no interaction of the jet and free stream above the plane of the jet exit. This location of the jet requires removal of the boundary layer from the vicinity of the jet exit, and it forces the free-stream streamline in the plane of the jet to be parallel to the free-stream direction. The series of photographs in figure 11 were taken with the jet located in a ground plane near the floor of the 7- by 10-foot test section to determine the effect of this location on the path of the jet wake. The experimental setup (fig. 2(b)) is similar to that used in reference 8 to prevent the boundary layer from forming in front of the jet exit. The results are presented for a range of effective velocity ratios from 0.10 to 0.24. Again, curves obtained from equation (1) are superimposed on the photographs. These data indicate that both the jet exiting from a ground board and the jet exiting away from the wind-tunnel walls give essentially the same jet wake path.

Jet Wake at $\delta_j \neq 90^\circ$

Although several investigators (refs. 8 to 12) have studied the path of the jet exiting perpendicular to the free stream, only a little experimental work (refs. 6 and 7) is published to describe the path of a jet inclined at large angles other than perpendicular to the free stream. This situation occurs in aircraft as they change angle of attack or as the thrust-producing device is deflected in transition flight. In the current investigation, the paths of jets were photographed at $\delta_j = 30^\circ$, 60°, 120°, 150°, and 180°. In all cases, the jet exit was located at the center of the wind-tunnel test section. To form a basis for comparison of these paths, equation (1) was extended to account for jet deflection. The slope of the deflected jet at its origin is given by

$$\frac{dx}{dz} = -\cot \delta_j \tag{2}$$

Integrating and nondimensionalizing by D gives the following equation when the effective velocity ratio is 0:

$$\frac{x}{D} = \frac{-z}{D} \cot \delta_j + C \tag{3}$$

To obtain the variation of the path with effective velocity ratio, the elements of equation (1) are combined with equation (3). In equation (1), the effective velocity ratio is based on the jet velocity being normal to free stream; for the deflected jet, the vertical component of jet velocity, $V_j \sin \delta_j$, is used. Combination of this change, equation (1), and equation (3) gives the following result:

$$\frac{x}{D} = -\frac{V_e^2}{4 \sin^2 \delta_j}\left(\frac{z}{D}\right)^3 - \frac{z}{D} \cot \delta_j \tag{4}$$

Since this empirical equation still gives the same result as equation (1) when δ_j is 90^o, it can be used for an arbitrary deflection angle. The curves superimposed on the photographs in figures 12 to 15 show the fit of this empirical equation.

The photographs of the wake for a jet exiting with a deflection of 30^o are presented in figure 12 for the effective velocity ratios ranging from 0.11 to 0.36. The photographs for the jet exiting with a deflection of 60^o are presented in figure 13 for effective velocity ratios ranging from 0.09 to 0.71. The curves computed with equation (4) provide a close fit to the path of the jet wake for both jet deflections less than 90^o through the range of effective velocity ratios.

The wake paths of a jet exiting at deflection angles into the free-stream direction ($\delta_j > 90^o$) are given next. The photographs for the path of a jet deflected 120^o are presented in figure 14 for effective velocity ratios ranging from 0.22 to 0.51. The photographs for the path of a jet deflected 150^o are presented in figure 15 for effective velocity ratios ranging from 0.19 to 0.50. The computed wake paths from equation (4) for the jet deflected 120^o show good agreement with the photographs. The computed paths for the jet deflected 150^o agree generally with the photographs for effective velocity ratios of 0.50 or greater. Below this effective velocity ratio, the initial penetration into the free stream, obtained from the empirical equation, is not as great as the photographed path. The resulting computed jet path does not show good agreement with the data for this range of effective velocity ratio.

The jet deflection angle of 180^o represents the extreme deflection of a jet into the wind. The photographs of this jet deflection are presented in figure 16 for effective velocity ratios ranging from 0.36 to 0.81. Since equation (4) equals infinity at this deflection angle, it is not applicable to these data, and there are no curves in figure 16. The maximum penetration of the jet wake upstream obtained from these photographs and from some additional runs at lower effective velocity ratios is presented in figure 17.

Summary of Available Data for Jet Path

Previous studies (refs. 6 to 12) have provided numerous theoretical and empirical expressions for the path of a jet inclined to the free stream. In this section, a number of these expressions are presented and then compared with equation (4) which is derived from the present data. Table I is a summary of the test conditions of the experimental investigations for comparison with the present paper.

Investigations reported by G. N. Abramovich (ref. 6).- Reference 6 presents two empirical equations. The first equation, obtained by G. S. Shandorov for jets whose temperature ranged from ambient to one-third of ambient and whose effective velocity ratio varied from 0.21 to 0.71, is

$$\frac{x}{D} = -V_e^2\left(\frac{z}{D}\right)^{2.55} - \frac{z}{D}\left(1 + V_e^2\right)\cot \delta_j \tag{5}$$

The second equation, obtained by Yu. V. Ivanov for jets whose effective velocity ratio varied from 0.03 to 0.29, is

$$\frac{x}{D} = -V_e 2.6\left(\frac{z}{D}\right)^3 - \frac{z}{D}\cot \delta_j \tag{6}$$

Investigation by G. S. Shandorov (ref. 7).- Reference 7 represents an analytic approach to the problem. This approach consists of finding the curvature of the jet axis by balancing the force caused by the pressure difference at the forward and back surfaces of a jet by a centrifugal force. (This solution is very similar to one proposed by M. S. Volinskiy and described in ref. 6.) The equation based on reference 7 is

$$\frac{x}{D} = -\frac{1}{6V_e^2}\left[\frac{\tan\frac{\delta_j}{2}}{e^{\left(3V_e^2\frac{z}{D}\right)}} + \frac{e^{\left(3V_e^2\frac{z}{D}\right)}}{\tan\frac{\delta_j}{2}} - \frac{2}{\sin\delta_j}\right] \tag{7}$$

Investigation by R. Jordinson (ref. 8).- Reference 8 presents data obtained with a jet mounted flush with a boundary-layer splitter plate. These data were used in references 2 and 15 to get empirical equations. The following equation from reference 2 is used to represent Jordinson's data:

$$\frac{x}{D} = -2.3V_e^3\left(\frac{z}{D}\right)^3 \tag{8}$$

Investigation by Callaghan and Ruggeri (ref. 10).- Reference 10 presents data obtained from a jet mounted flush with the wind-tunnel wall. The air from the jet was heated to approximately 400° F (204° C) by passing through an electric heater. The following equation is obtained from this reference:

$$\frac{x}{D} = -0.118\left(\frac{\rho_\infty V_\infty}{\rho_j V_j}\right)^2\left(\frac{z}{D}\right)^{3.3} \tag{9}$$

Investigation by K. R. Storms (ref. 11).- Reference 11 presents an equation for a jet deflection angle of 90° which was modified so that it would be compatible with the other equations used in this report. Use of the nominal value of the velocity ratio instead of the corrected velocity ratio changes the constant in the equation from 0.13 to 0.195 and gives the following equation:

$$\frac{x}{D} = -0.195V_e^2\left(\frac{z}{D}\right)^3 \tag{10}$$

In contrast to the other references (refs. 6 to 10 and 12), the results of this investigation were obtained with the jet exiting at several locations relative to the wind-tunnel wall. In addition to a jet located flush with the wall, the jet was also located out in the free stream at distances of 0.2 and 0.4 of the wind-tunnel test-section height away from the nearest wind-tunnel wall.

COMPARISON OF JET PATHS FROM VARIOUS INVESTIGATIONS

A comparison of jet paths for a deflection angle of 90° is presented in figure 18. These data show that the scatter among the different results appears large; however, when they are compared with the appropriate photographs in figure 6, all the jet paths but those of reference 7 fall within the jet wake vapor. The analytic calculation (Shandorov, ref. 7) does not follow a consistent variation in path when compared with the empirical and experimental results and predicts more penetration at effective velocity ratios below 0.167.

The comparisons for deflection angles of 30° and 60° are presented in figures 19 and 20, respectively. These results of the various studies are in very close agreement; this is illustrated when the results are compared with the photographs in figures 12 ($\delta_j = 30°$) and 13 ($\delta_j = 60°$). It should be noted that the analytic expression (Shandorov, ref. 7, eq. (7)) agrees with the empirical results of the present investigation at jet deflection angles less than 90°. It should also be noted that the only experimental data presented in reference 7 are for a deflection angle of 60°. This fact and these comparisons imply that this expression is applicable only for a limited range of deflection angles near 60°.

The comparisons for a deflection angle of 120° are presented in figure 21. The empirical results from reference 6 (Shandorov, eq. (5), and Ivanov, eq. (6)) show very close agreement with the photographs in figure 14. However, as at the 90° deflection, the analytic calculation (ref. 7, Shandorov, eq. (7)) does not follow a consistent variation in path compared with the empirical and experimental results.

The comparisons for a deflection angle of 150° are presented in figure 22. The analytic equation (ref. 7, Shandorov, eq. (7)) again shows much greater penetration of the free stream than the corresponding photographs in figure 15. This is further indication that this analytic procedure is valid only for a limited range of jet deflection angles near 60°. The empirical results from reference 6 (Shandorov, eq. (5), and Ivanov, eq. (6)) provide closer agreement than equation (4) for the photographs in figure 15. There is one significant difference between these two equations from reference 6. Equations (5) and (6) give the following slopes at the jet exit, respectively,

$$\left.\begin{aligned} \frac{dx}{dz} &= -\left(1 + V_e^2\right) \cot \delta_j \\ \frac{dx}{dz} &= -\cot \delta_j \end{aligned}\right\} \tag{11}$$

Comparison shows that the initial slope from equation (5) becomes too large as the effective velocity ratio increases whereas the initial slope from equation (6) is a function only of deflection angle. (See fig. 22(d) for the best example of slope error from eq. (5).) For all the conditions examined in these figures (figs. 18 to 22), equation (4) provides a good fit to most of the data presented. This equation, however, failed to give a good fit at a deflection angle of 150° when the effective velocity ratio was below 0.50. Equation (6) (Ivanov, ref. 6) does provide a good fit at a deflection angle of 150° as well as at most of the other deflection angles.

CONCLUSIONS

An investigation of the general path of the wake from a single jet exiting at large angles to the free stream gives the following results:

1. The jet paths from the photographs of the air mixed with water give essentially the same results when the jet is exiting upward or downward as well as when the jet is located adjacent to a large surface or located away from adjacent surfaces.

2. The primary variables determining the jet path from a particular nozzle are the deflection angle of the nozzle exit and the effective velocity ratio (square root of the ratio of free-stream dynamic pressure to jet dynamic pressure).

3. The empirical equation developed in the present paper provided a good fit to most of the jet paths photographed. This equation, however, failed to give a good fit at a deflection angle of 150° when the effective velocity ratio was below 0.50. The empirical equation developed by Yu. V. Ivanov (Abramovich, G. N.: The Theory of Turbulent Jets.

M.I.T. Press, c.1963, p. 544) provided a good fit at a deflection angle of 150^{o} as well as at most of the other deflections considered.

Langley Research Center,
National Aeronautics and Space Administration,
Langley Station, Hampton, Va., July 31, 1968,
721-01-00-18-23.

REFERENCES

1. Margason, Richard J.: Jet-Induced Effects in Transition Flight. Conference on V/STOL and STOL Aircraft, NASA SP-116, 1966, pp. 177-189.

2. Williams, John; and Wood, Maurice N.: Aerodynamic Interference Effects With Jet-Lift V/STOL Aircraft Under Static and Forward-Speed Conditions. Tech. Rep. No. 66403, Brit. R.A.E., Dec. 1966.

3. Chang-Lu, Hsiu-Chen: Aufrollung Eines Zylindrischen Strahles Durch Querwind (Rollup of a Cylindrical Jet in a Crosswind). Doctorial Dissertation, Univ. of Göttingen, 1942.

4. Lee, C. C.: A Review of Research on the Interaction of a Jet With an External Stream. Tech. Note R-184 (Contract No. DA-01-021-AMC-11528(z)), Res. Lab., Brown Engineering Co., Inc., Mar. 1966. (Available from DDC as AD 630 294.)

5. Garner, Jack E.: A Review of Jet Efflux Studies Applicable to V/STOL Aircraft. AEDC-TR-67-163, U.S. Air Force, Sept. 1967. (Available from DDC as AD 658 432.)

6. Abramovich, G. N.: The Theory of Turbulent Jets. M.I.T. Press, C. 1963, pp. 541-552.

7. Shandorov, G. S.: Calculation of a Jet Axis in a Drifting Flow. NASA TT F-10,638, 1966.

8. Jordinson, R.: Flow in a Jet Directed Normal to the Wind. R. & M. No. 3074, British A.R.C., 1958.

9. Keffer, J. F.; and Baines, W. D.: The Round Turbulent Jet in a Cross-Wind. J. Fluid Mech., vol. 15, pt. 4, Apr. 1963, pp. 481-497.

10. Callaghan, Edmund E.; and Ruggeri, Robert S.: Investigation of the Penetration of an Air Jet Directed Perpendicularly to an Air Stream. NACA TN 1615, 1948.

11. Storms, Kenneth R.: Low-Speed Wind Tunnel Investigation of a Jet Directed Normal to the Wind. Rep. 885, Aeronaut. Lab., Univ. of Washington, Nov. 1965.

12. Hardy, William G. S.: Non-Parallel Flow Interactions. M.A.E. Thesis, Univ. of Virginia, 1967.

13. Kirkpatrick, David L. I.: Wind-Tunnel Corrections for V/STOL Model Testing. M.A.E. Thesis, Univ. of Virginia, 1962.

14. Mechtly, E. A.: The International System of Units—Physical Constants and Conversion Factors. NASA SP-7012, 1964.

15. Monical, Richard E.: A Method of Representing Fan-Wind Combinations for Three-Dimensional Potential Flow Solutions. J. Aircraft, vol. 2, no. 6, Nov.-Dec. 1965, pp. 527-530.

TABLE I.- SUMMARY OF TEST CONDITIONS FOR THE PRESENT INVESTIGATION AND FOR THE EXPERIMENTAL INVESTIGATIONS IN REFERENCES 6 AND 8 TO 12

Investigation		Wind-tunnel size, height × width		Jet location, fraction of wind-tunnel height	Jet diameter		p_j/p_∞	T_j/T_∞	V_e	δ_j, deg	Method of path determination
Reference	Equation in present paper	ft	m		in.	cm					
Present paper	4	7 × 10	2.13 × 3.05	0 and 0.5	1.0	2.54	1.1 to 2.0	1.00	0.10 to 0.85	30 to 180	Water-vapor flow visualization
6	5	----------	----------	0	0.79	2.00	--------	0.33 to 1.00	0.21 to 0.71	45 to 90	----------
6	6	----------	----------	----------	----------	----------	--------	1.00	0.03 to 0.29	60 to 120	----------
8	8	5 × 1	1.52 × 0.30	0	0.5 and 1.0	1.27 and 2.54	--------	1.00	0.125 to 0.25	90	Pressure measurement
9	None	4 × 8	1.22 × 2.44	0	0.375	0.95	Slightly above 1.0	1.00	0.10 to 0.5	90	Hot-wire anemometer and smoke flow visualization
10	9	1.67 × 0.17	0.51 × 0.05	0	0.250 to 0.625	0.64 to 1.59	1.2 to 2.7	1.90	0.14 to 0.5	90	Pressure measurement
11	10	2.5 hexagon	0.76 hexagon	0, 0.2, and 0.4	0.55	1.40	--------	1.00	0.10 to 0.25	90	Pressure measurement
12	See reference	0.69 × 1.0	0.21 × 0.30	0	0.25	0.64	--------	1.00	0.10 to 0.25	90	Smoke flow visualization

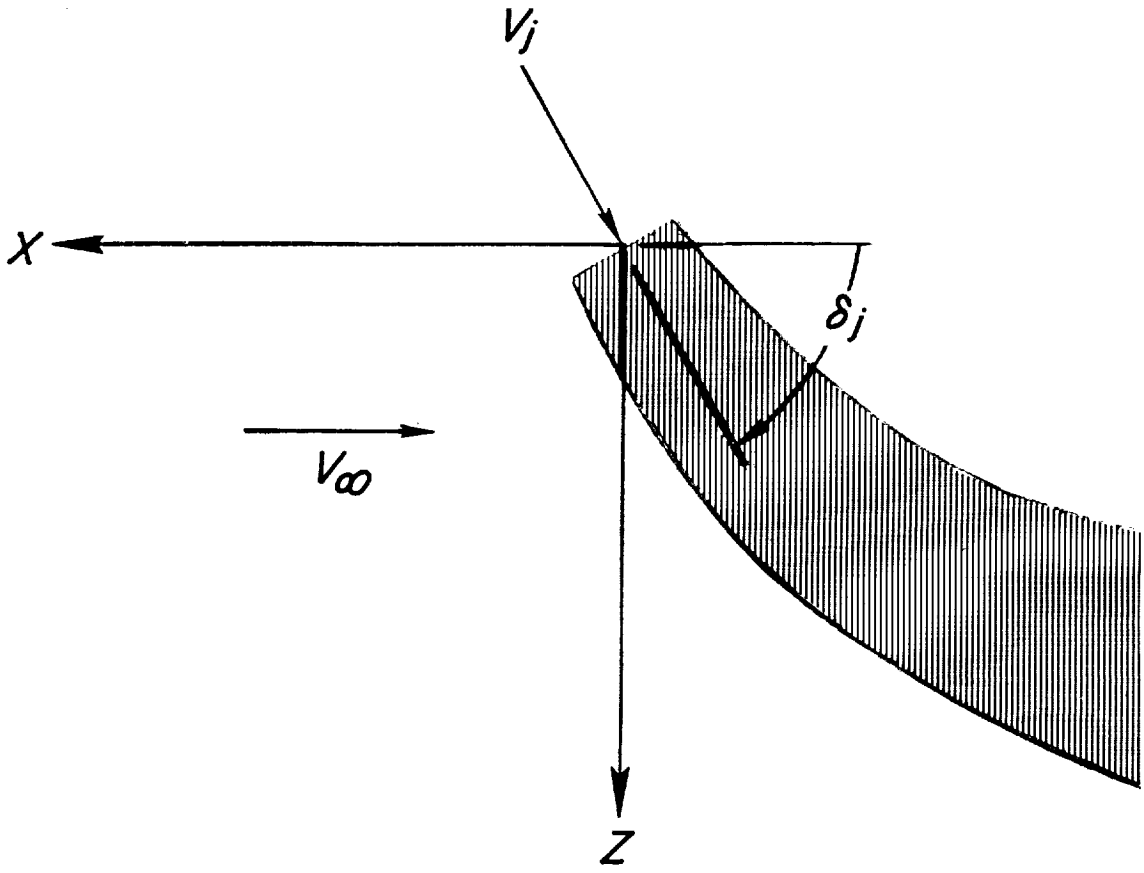

Figure 1.- Positive sense of directions, velocities, and jet deflection angle.

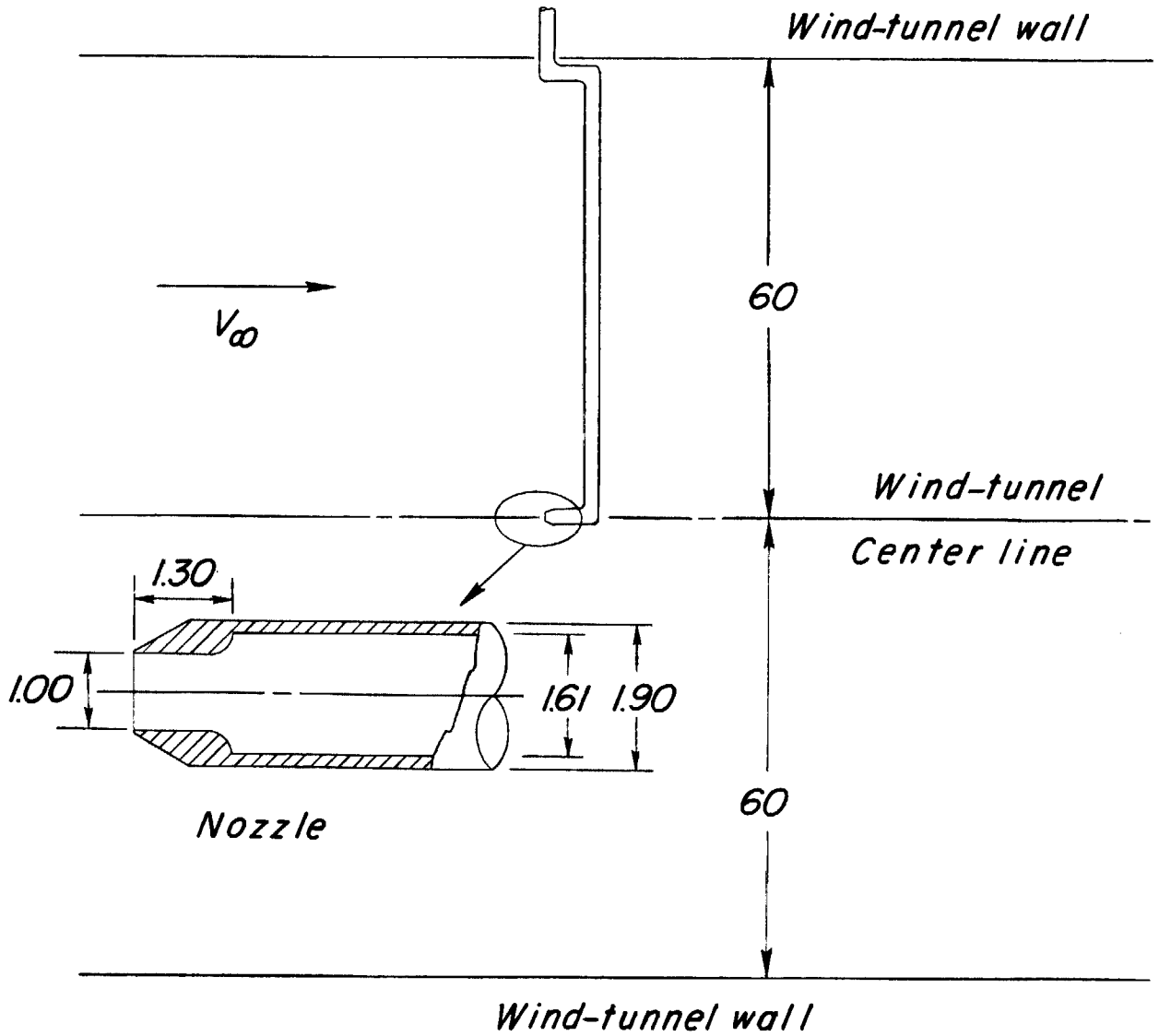

(a) Plan view of compressed-air and water-vapor supply pipe installed with nozzle in center of wind tunnel at deflection of 180°. Also shown is section view of nozzle.

Figure 2.- Drawings of nozzle in wind tunnel. All dimensions are nondimensionalized by nozzle diameters.

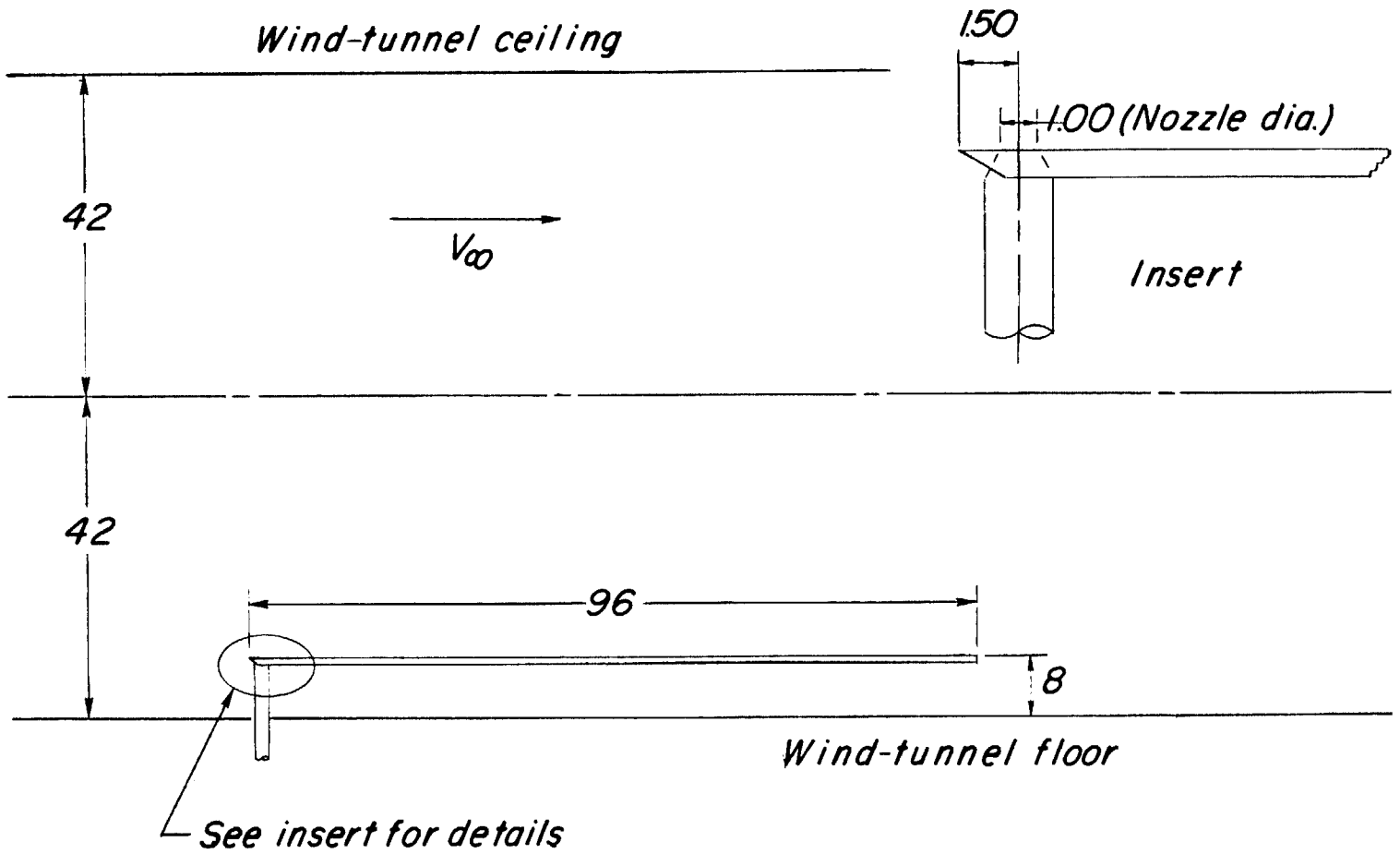

(b) Side view of nozzle installed through ground plane.

Figure 2.- Concluded.

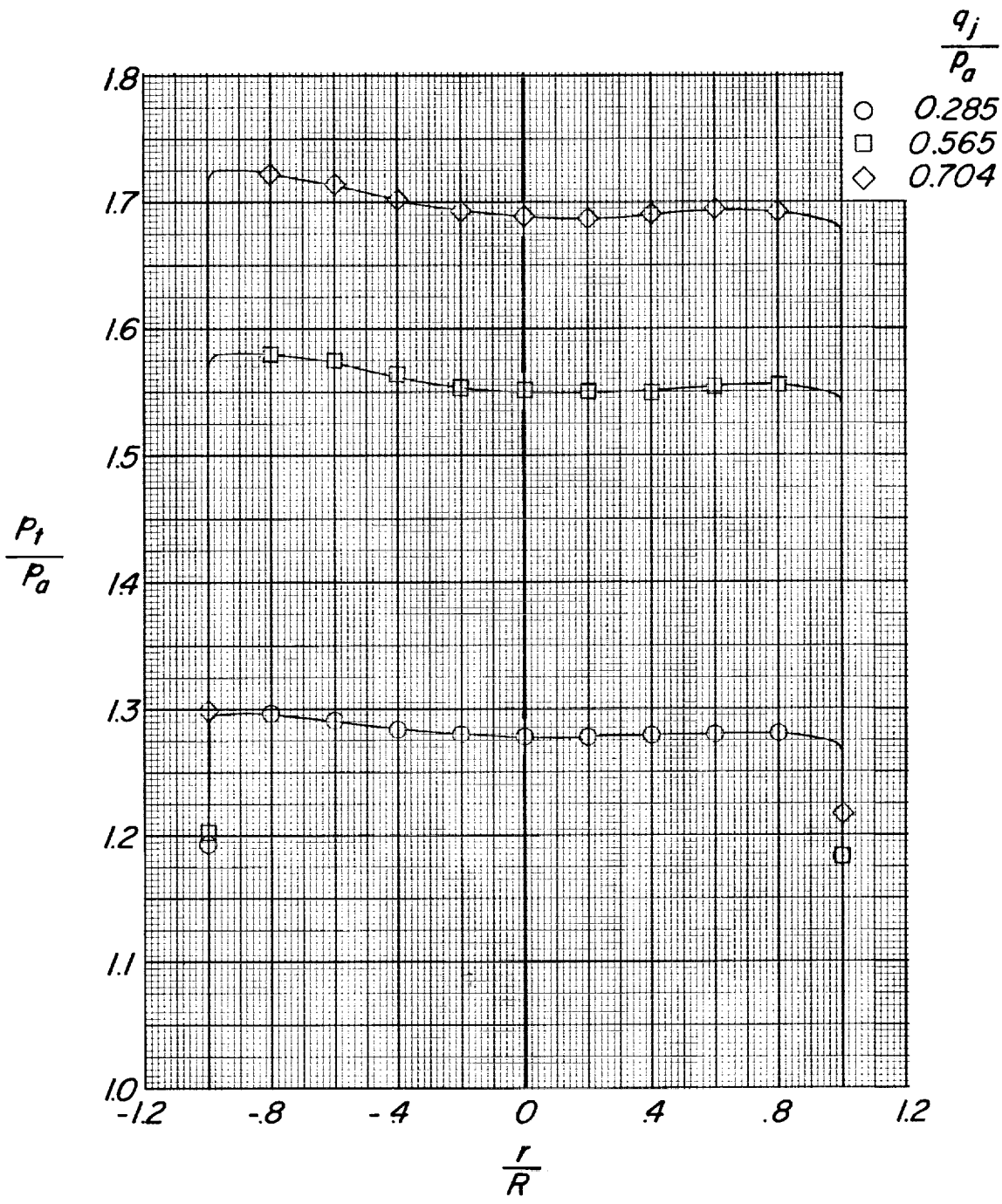

Figure 3.- Exit pressure profiles showing distribution of total pressure across nozzle diameter at three jet dynamic pressures.

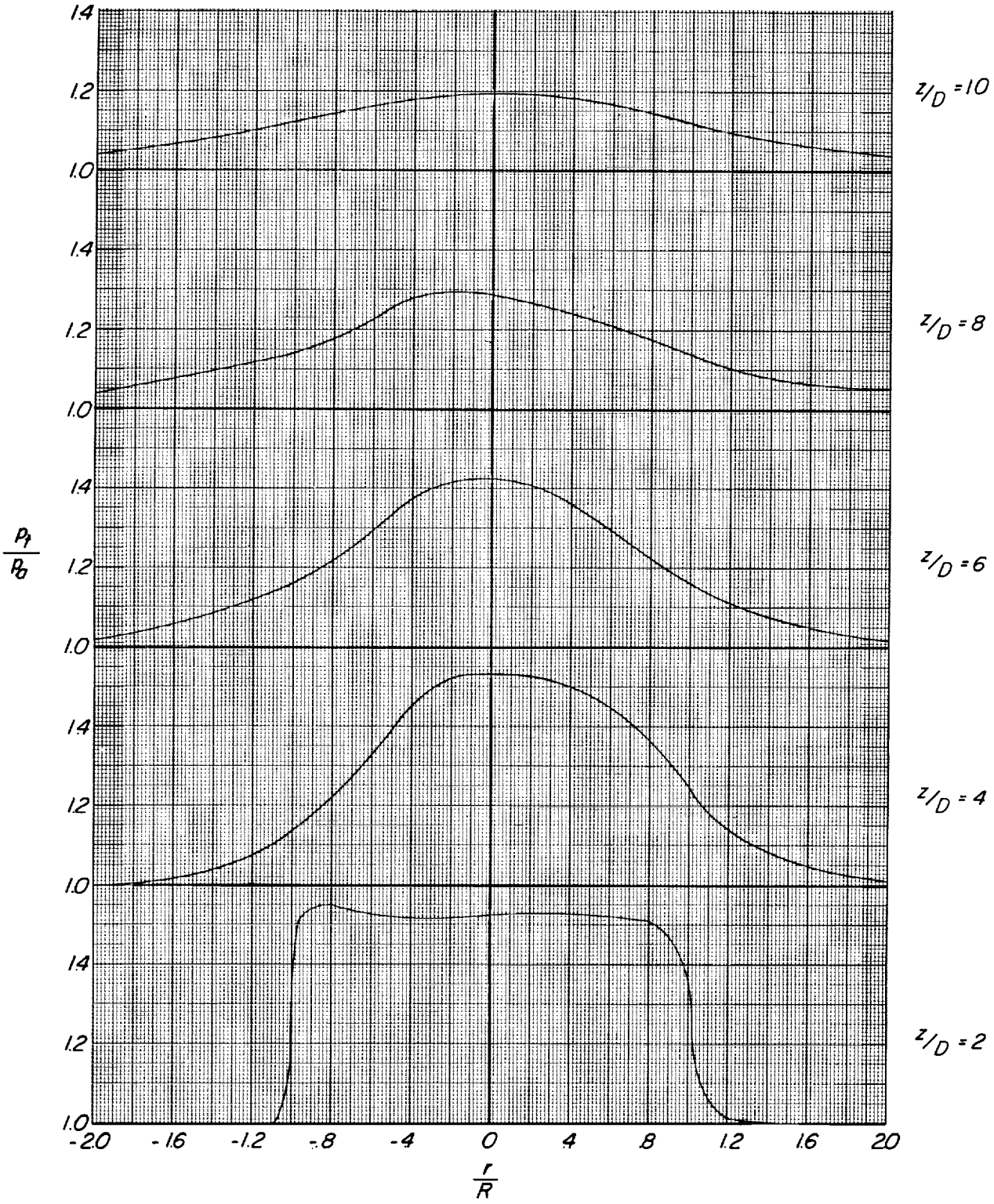

Figure 4.- Pressure profiles of jet exhausting into ambient air at several locations downstream from nozzle.

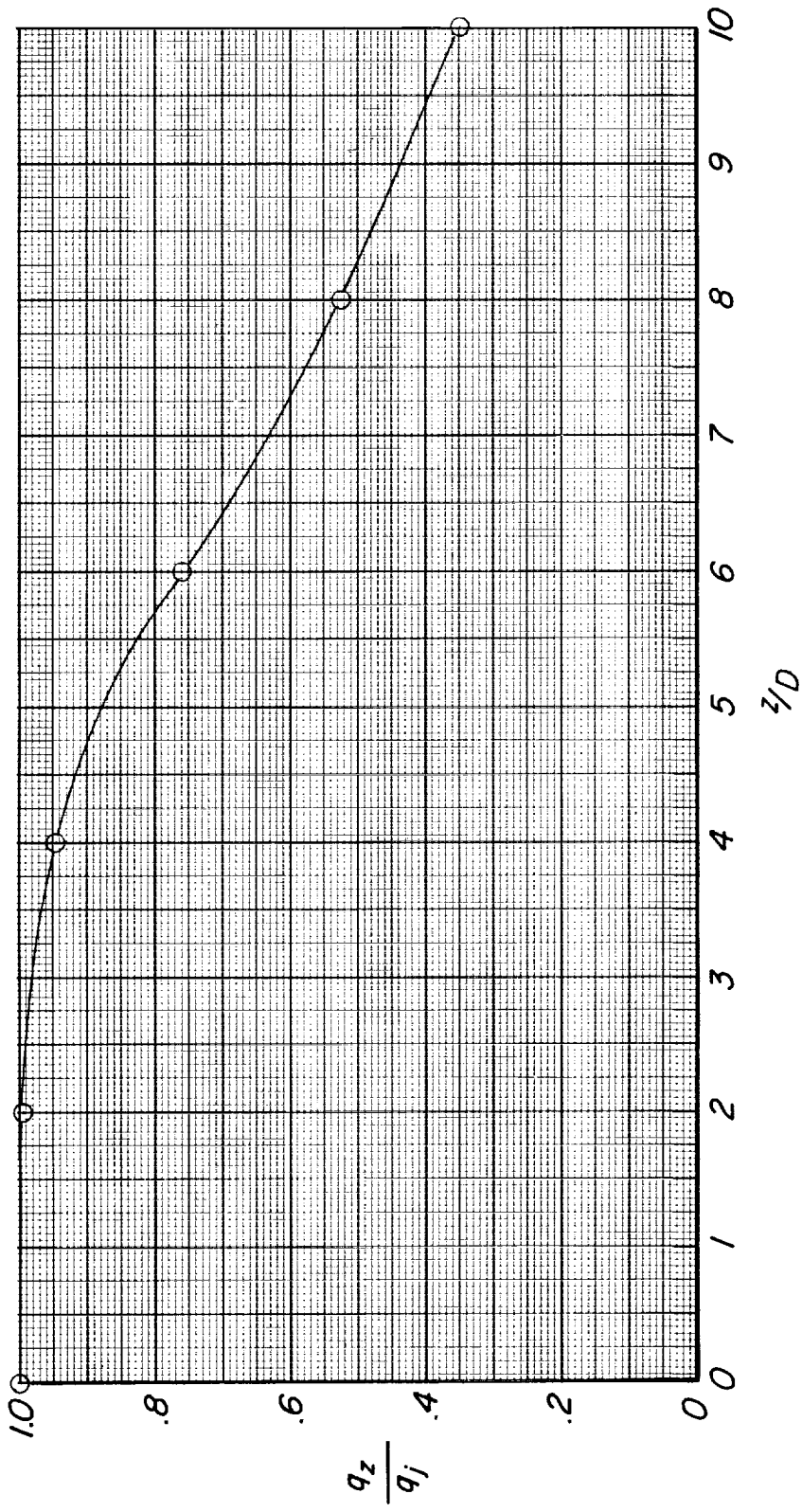

Figure 5.- Variation of peak dynamic pressure with downstream distance.

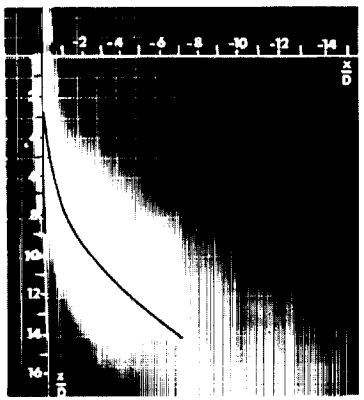

(a) $V_e = 0.099$; $q_j/p_a = 0.569$.

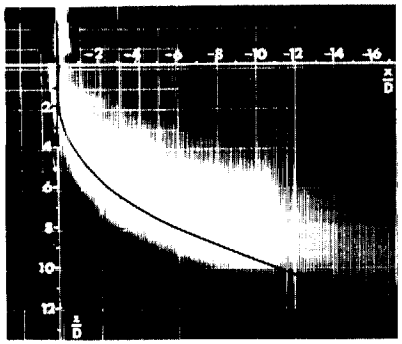

(b) $V_e = 0.212$; $q_j/p_a = 0.212$.

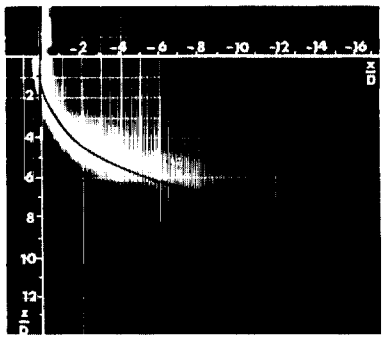

(c) $V_e = 0.311$; $q_j/p_a = 0.270$.

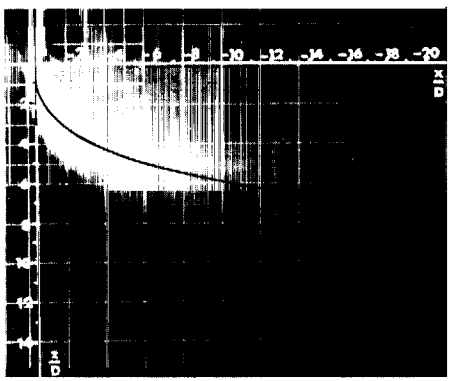

(d) $V_e = 0.421$; $q_j/p_a = 0.222$.

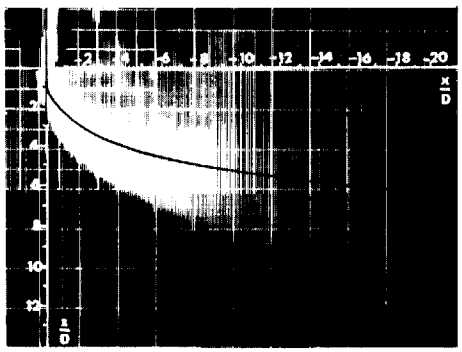

(e) $V_e = 0.568$; $q_j/p_a = 0.123$.

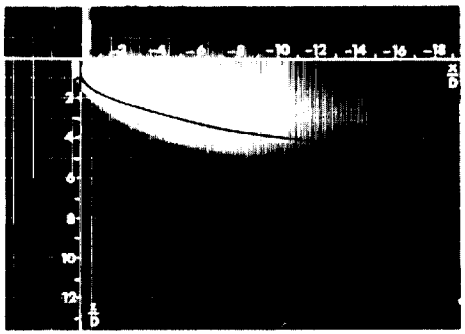

(f) $V_e = 0.832$; $q_j/p_a = 0.077$.

Figure 6.- Jet wake path for nozzle exiting downward in middle of wind tunnel at several effective velocity ratios. $\delta_j = 90^0$.

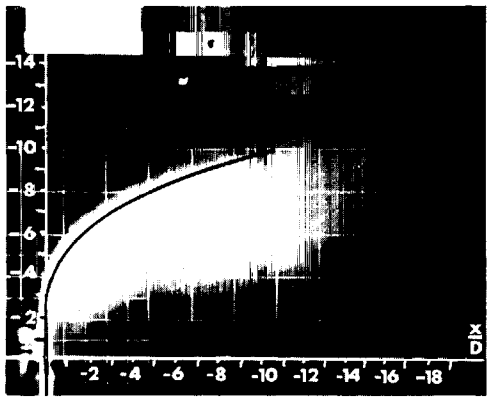

(a) $V_e = 0.210$; $q_j/p_a = 0.589$.

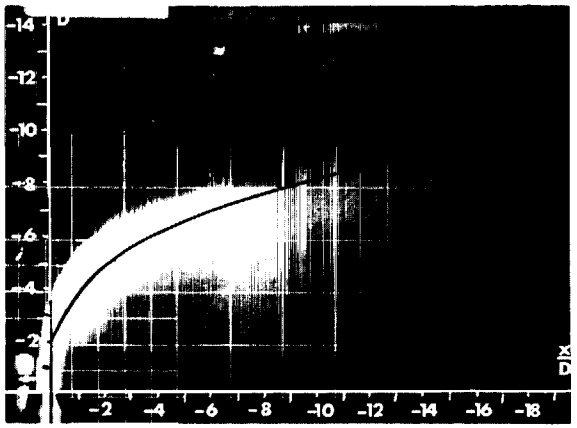

(b) $V_e = 0.267$; $q_j/p_a = 0.370$.

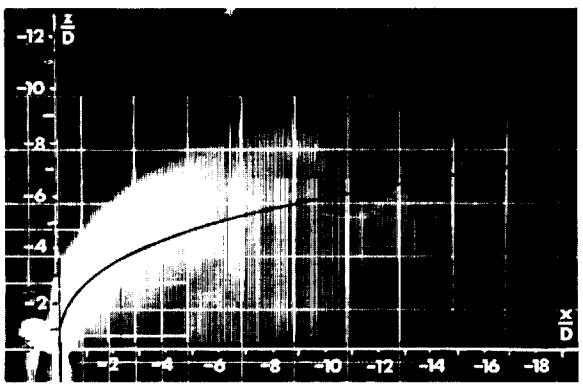

(c) $V_e = 0.466$; $q_j/p_a = 0.121$.

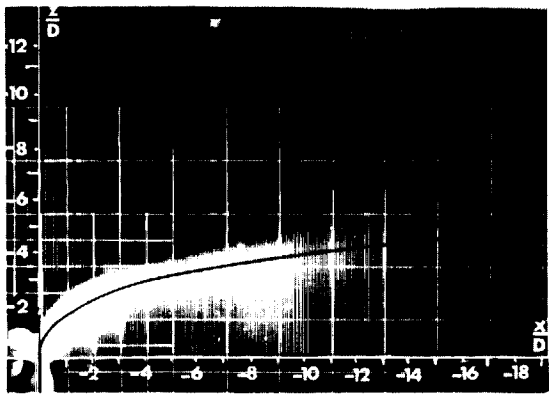

(d) $V_e = 0.846$; $q_j/p_a = 0.037$.

Figure 7.- Jet wake path for nozzle exiting upward in middle of wind tunnel at several effective velocity ratios. $\delta_j = 90^o$.

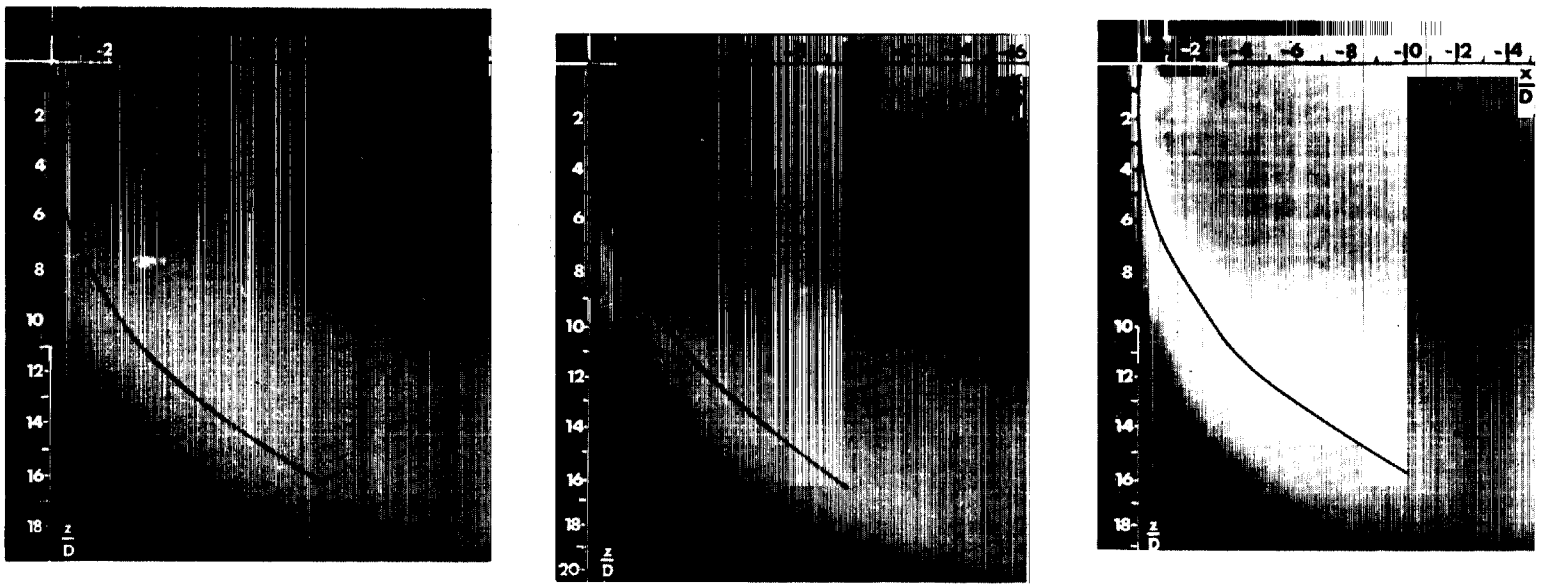

(a) $q_\infty/p_a = 0.0068$; $q_j/p_a = 0.658$.

(b) $q_\infty/p_a = 0.0034$; $q_j/p_a = 0.344$.

(c) $q_\infty/p_a = 0.0017$; $q_j/p_a = 0.171$.

Figure 8.- Jet wake path for nozzle exiting downward in middle of wind tunnel at effective velocity ratio of 0.10 for several combinations of free-stream dynamic pressure and jet dynamic pressure. $\delta_j = 90^0$.

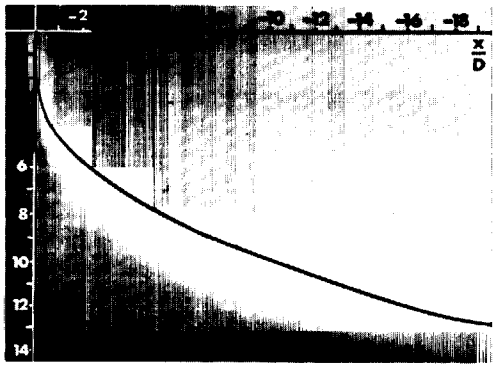

(a) $q_\infty/p_a = 0.0270$; $q_j/p_a = 0.669$.

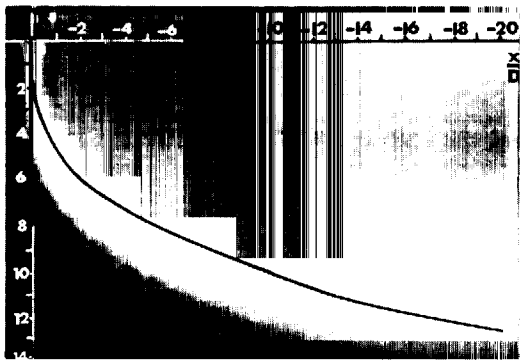

(b) $q_\infty/p_a = 0.0136$; $q_j/p_a = 0.348$.

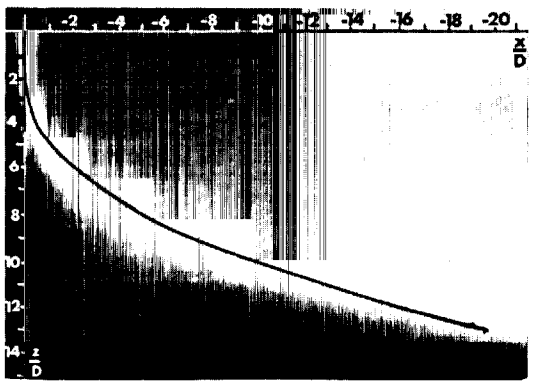

(c) $q_\infty/p_a = 0.0068$; $q_j/p_a = 0.173$.

Figure 9.- Jet wake path for nozzle exiting downward in middle of wind tunnel at effective velocity ratio of 0.20 for several combinations of free-stream dynamic pressure and jet dynamic pressure. $\delta_j = 90^0$.

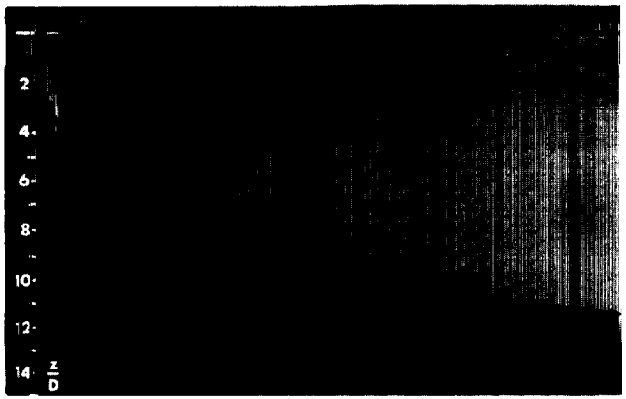

(a) $q_\infty/p_a = 0.0420$; $q_j/p_a = 0.676$.

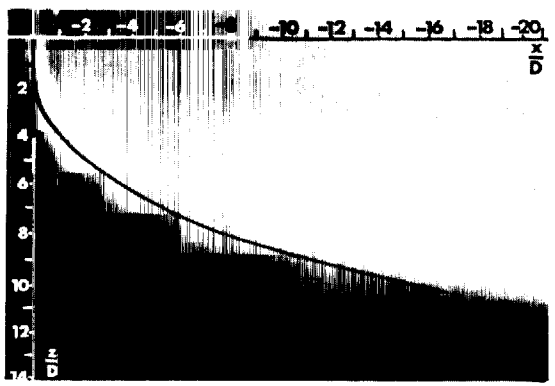

(b) $q_\infty/p_a = 0.0211$; $q_j/p_a = 0.351$.

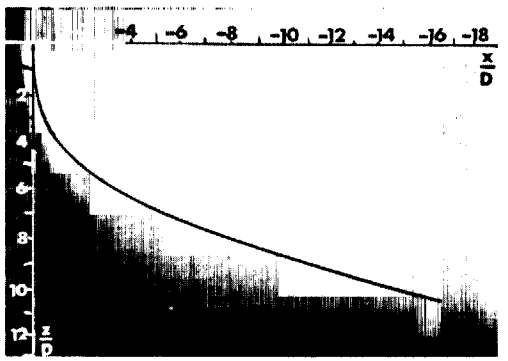

(c) $q_\infty/p_a = 0.0107$; $q_j/p_a = 0.174$.

Figure 10.- Jet wake path for nozzle exiting downward in middle of wind tunnel at effective velocity ratio of 0.25 for several combinations of free-stream dynamic pressure and jet dynamic pressure. $\delta_j = 90^0$.

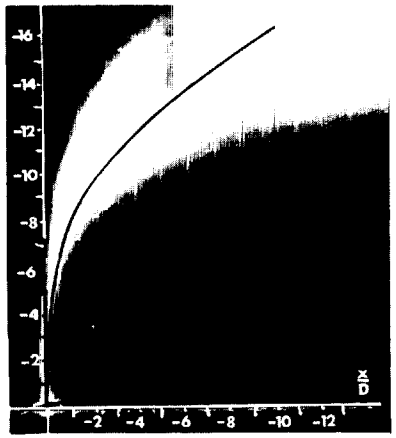

(a) $V_e = 0.099$; $q_j/p_a = 0.342$.

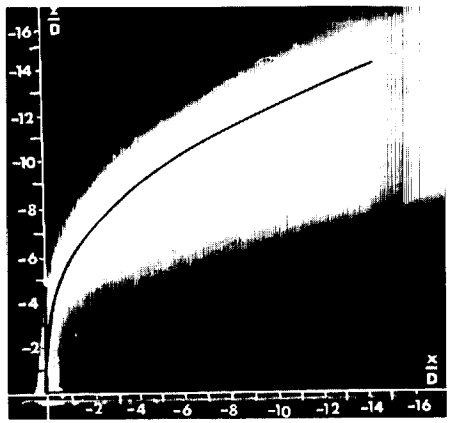

(b) $V_e = 0.149$; $q_j/p_a = 0.345$.

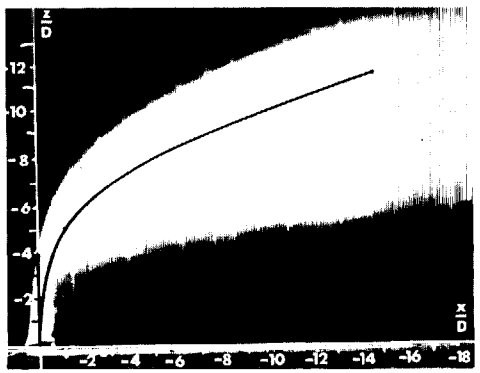

(c) $V_e = 0.197$; $q_j/p_a = 0.350$.

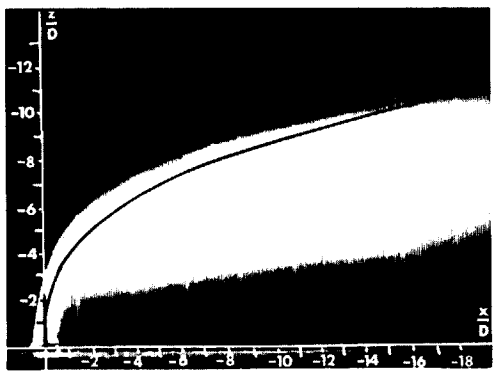

(d) $V_e = 0.244$; $q_j/p_a = 0.355$.

Figure 11.- Jet wake path for nozzle exiting upward through ground plane at several effective velocity ratios. $\delta_j = 90^0$.

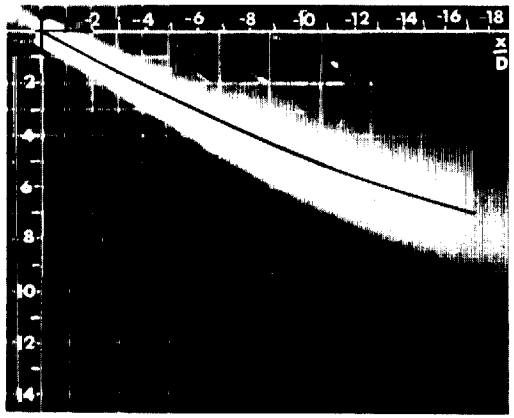

(a) $V_e = 0.113$; $q_j/p_a = 0.541$.

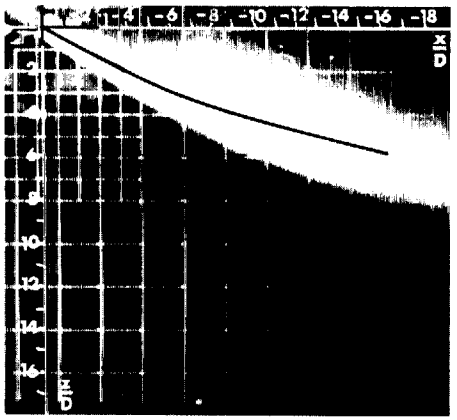

(b) $V_e = 0.179$; $q_j/p_a = 0.553$.

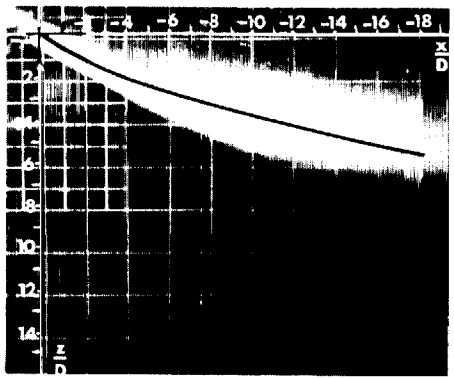

(c) $V_e = 0.235$; $q_j/p_a = 0.547$.

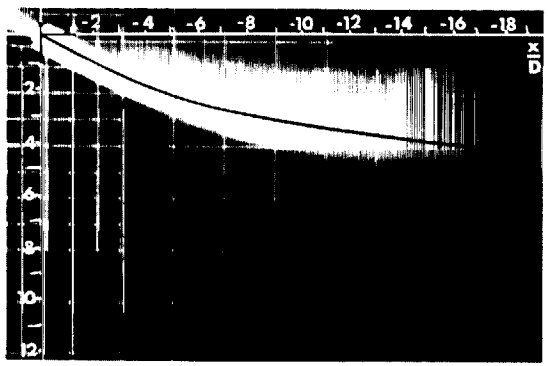

(d) $V_e = 0.356$; $q_j/p_a = 0.601$.

Figure 12.- Jet wake path for nozzle exiting downward in middle of wind tunnel at several effective velocity ratios. $\delta_j = 30^o$.

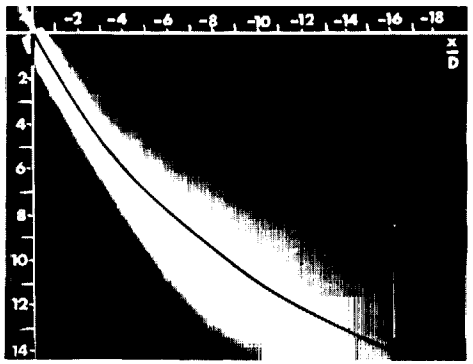

(a) $V_e = 0.092$; $q_j/p_a = 0.568$.

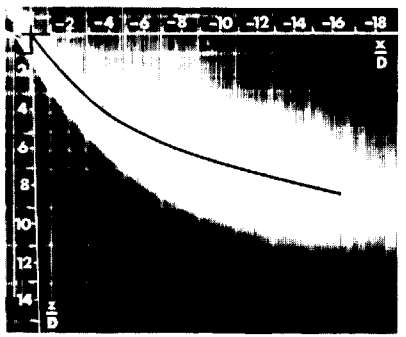

(b) $V_e = 0.225$; $q_j/p_a = 0.609$.

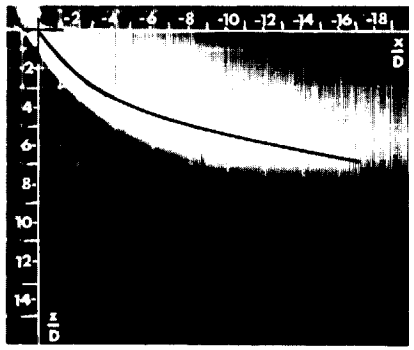

(c) $V_e = 0.353$; $q_j/p_a = 0.609$.

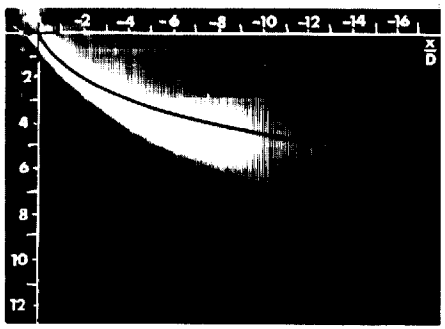

(d) $V_e = 0.513$; $q_j/p_a = 0.287$.

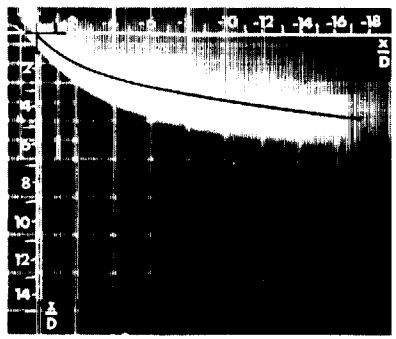

(e) $V_e = 0.712$; $q_j/p_a = 0.149$.

Figure 13.- Jet wake path for nozzle exiting downward in middle of wind tunnel at several effective velocity ratios. $\delta_j = 60^0$.

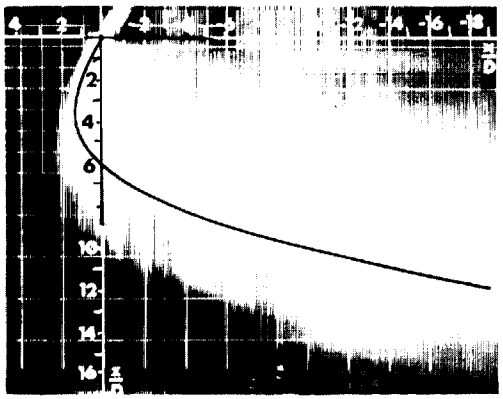

(a) $V_e = 0.216$; $q_j/p_a = 0.560$.

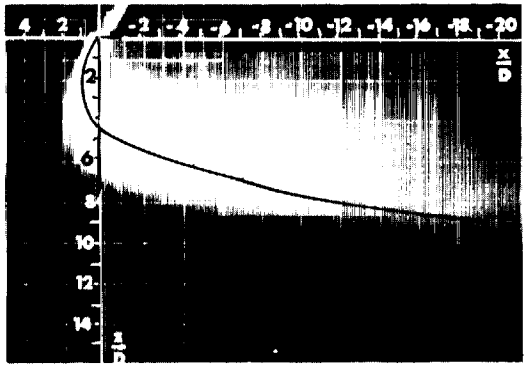

(b) $V_e = 0.309$; $q_j/p_a = 0.274$.

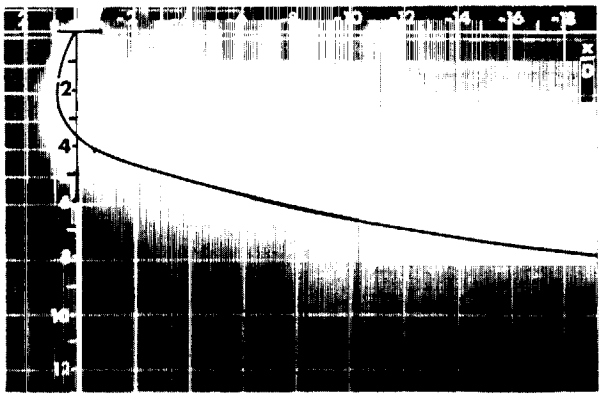

(c) $V_e = 0.375$; $q_j/p_a = 0.185$.

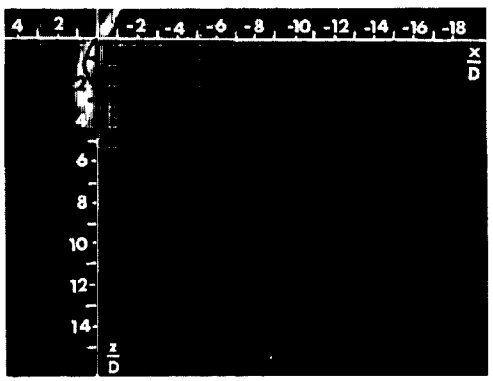

(d) $V_e = 0.511$; $q_j/p_a = 0.100$.

Figure 14.- Jet wake path for nozzle exiting downward in middle of wind tunnel at several effective velocity ratios. $\delta_j = 120^0$.

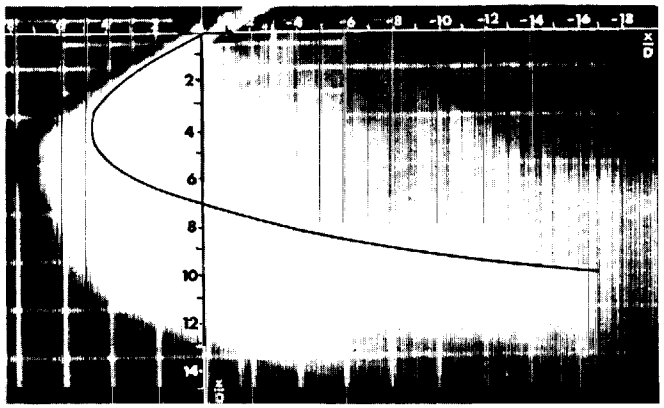

(a) $V_e = 0.186$; $q_j/p_a = 0.564$.

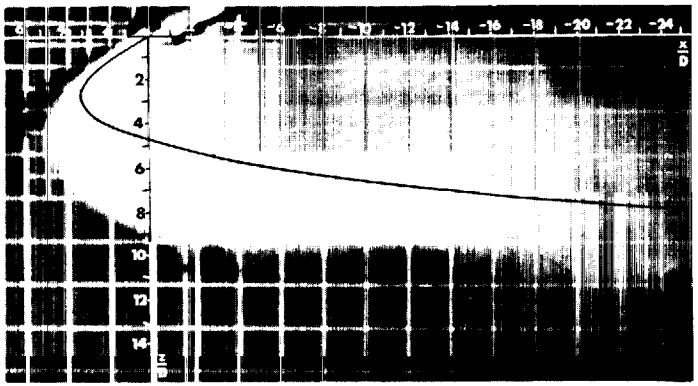

(b) $V_e = 0.273$; $q_j/p_a = 0.262$.

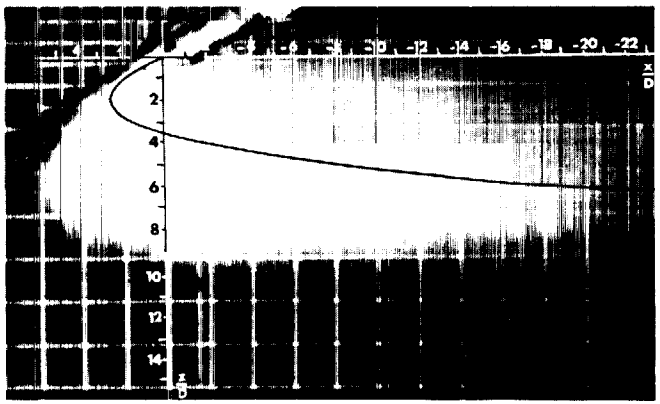

(c) $V_e = 0.372$; $q_j/p_a = 0.187$.

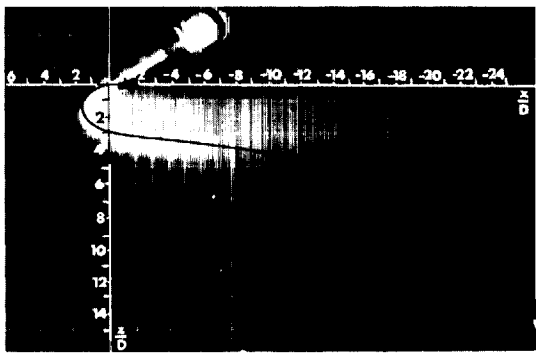

(d) $V_e = 0.500$; $q_j/p_a = 0.159$.

Figure 15.- Jet wake path for nozzle exiting downward in middle of wind tunnel at several effective velocity ratios. $\delta_j = 150^o$.

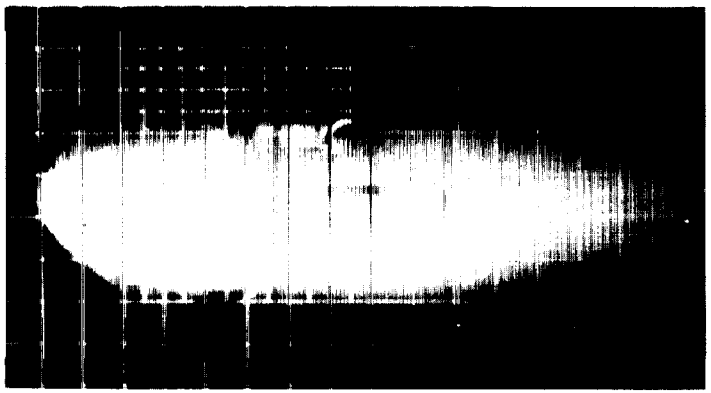

(a) $V_e = 0.355$; $q_j/p_a = 0.603$.

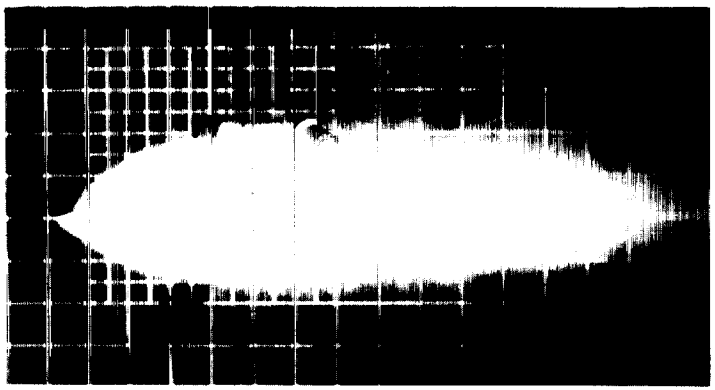

(b) $V_e = 0.479$; $q_j/p_a = 0.330$.

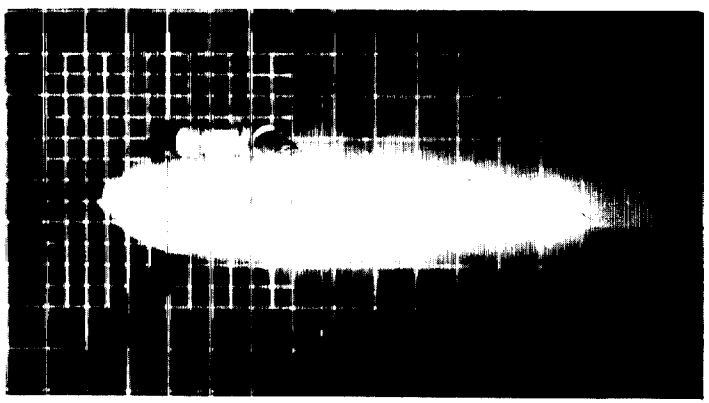

(c) $V_e = 0.607$; $q_j/p_a = 0.206$.

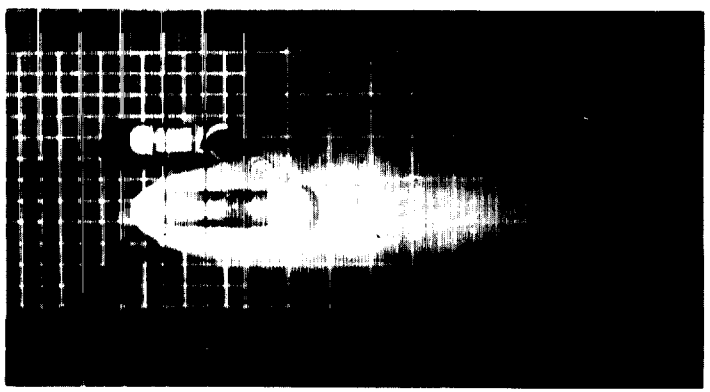

(d) $V_e = 0.807$; $q_j/p_a = 0.116$.

Figure 16.- Jet wake penetration for nozzle exiting into free stream ($\delta_j = 180^0$) in middle of wind tunnel at several effective velocity ratios.

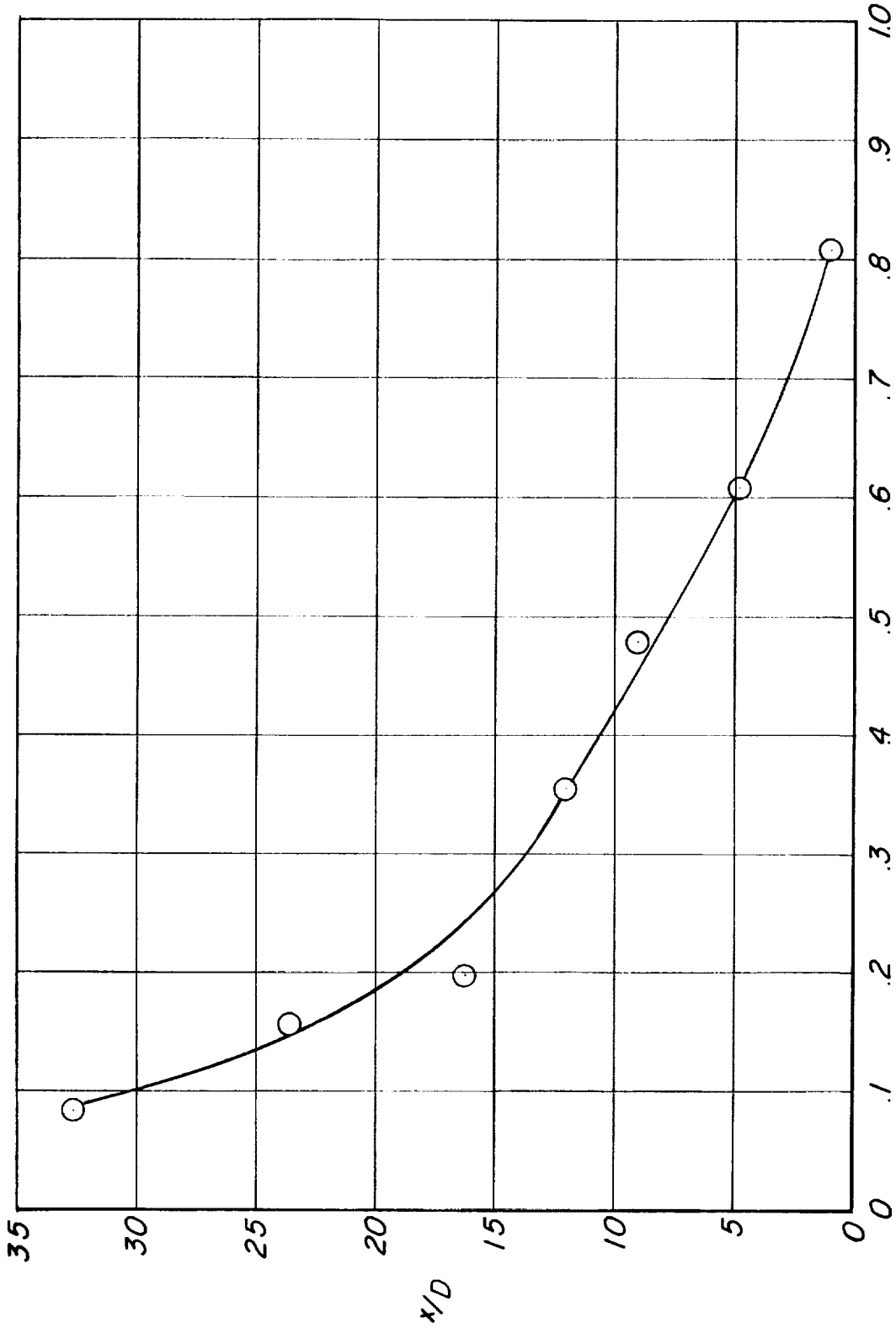

Figure 17.- Maximum penetration of jet wake upstream as a function of effective velocity ratio. $\delta_j = 180^0$.

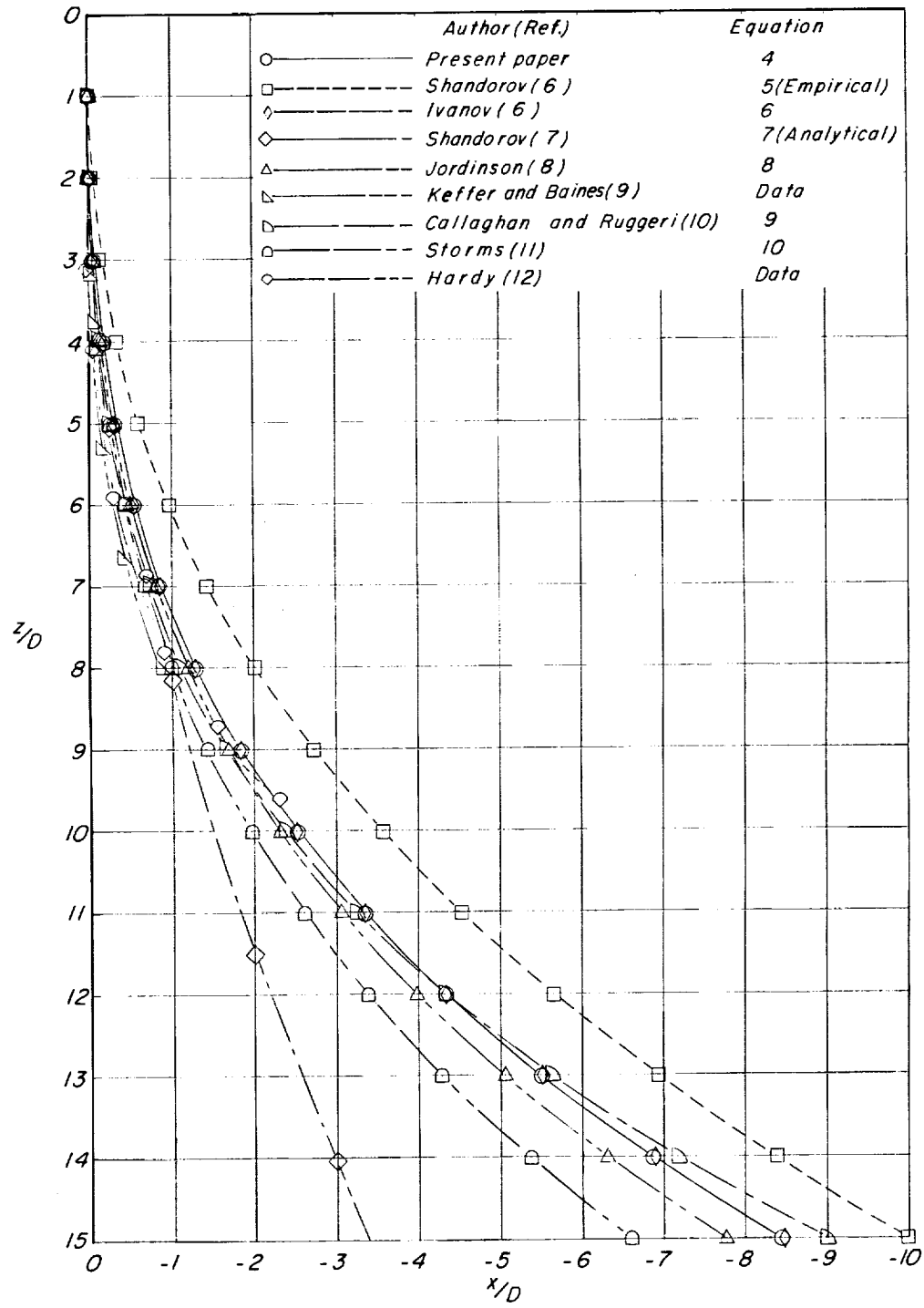

(a) $V_e = 0.100$.

Figure 18.- Comparison of jet wake path from equation (4) with results from references 6 to 12 at several effective velocity ratios. $\delta_j = 90^o$.

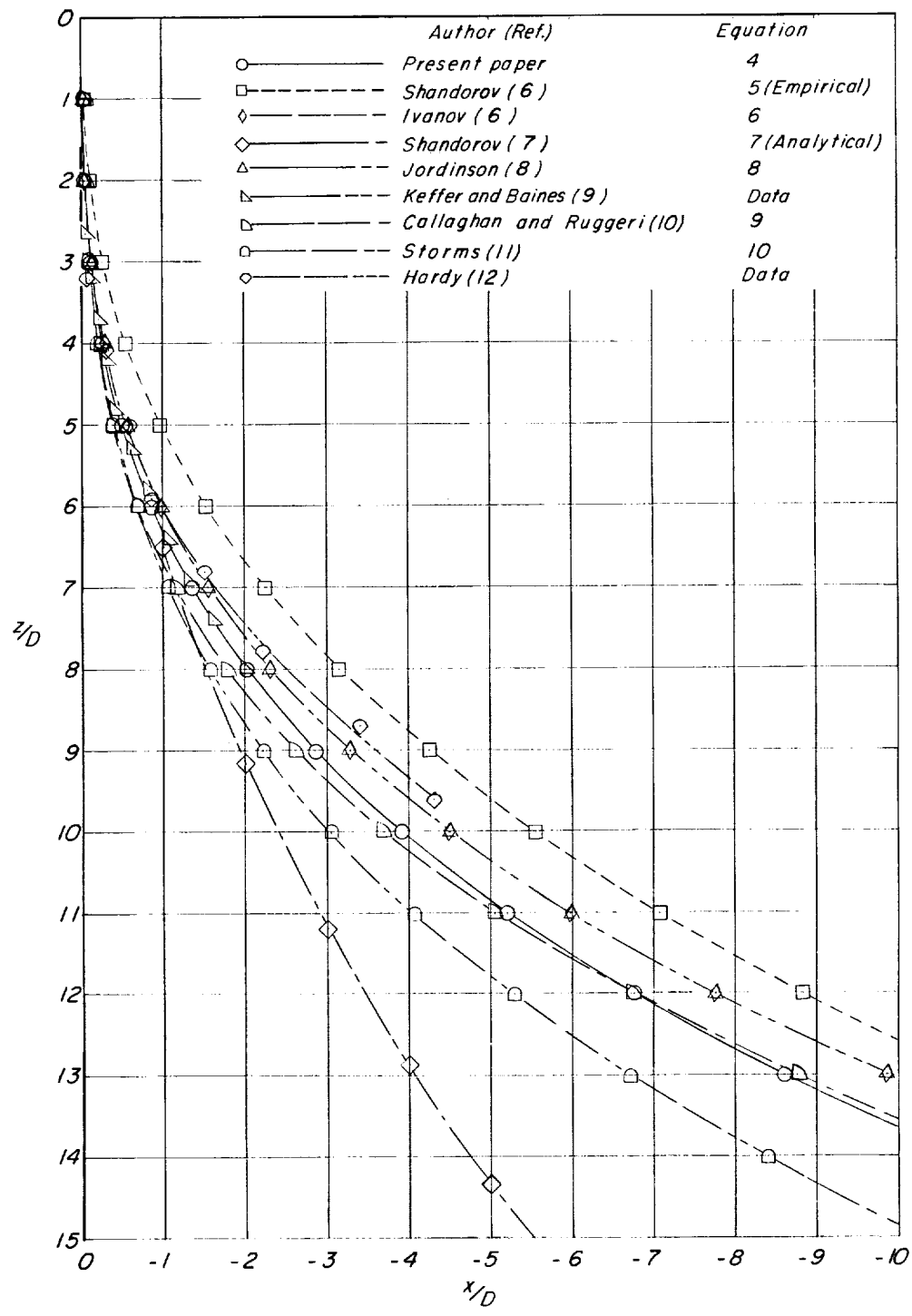

(b) $V_e = 0.125$.

Figure 18.- Continued.

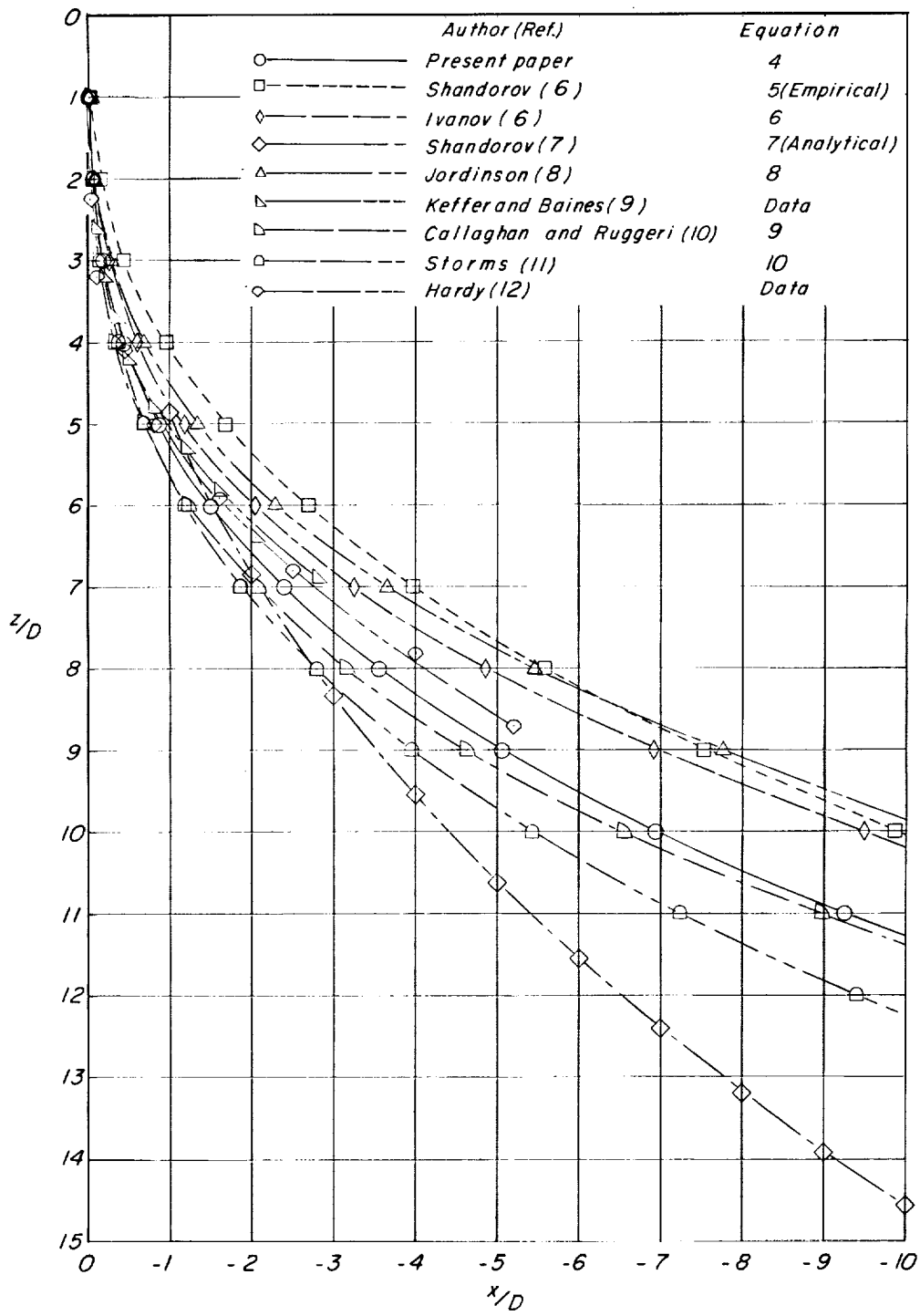

(c) $V_e = 0.167$.

Figure 18.- Continued.

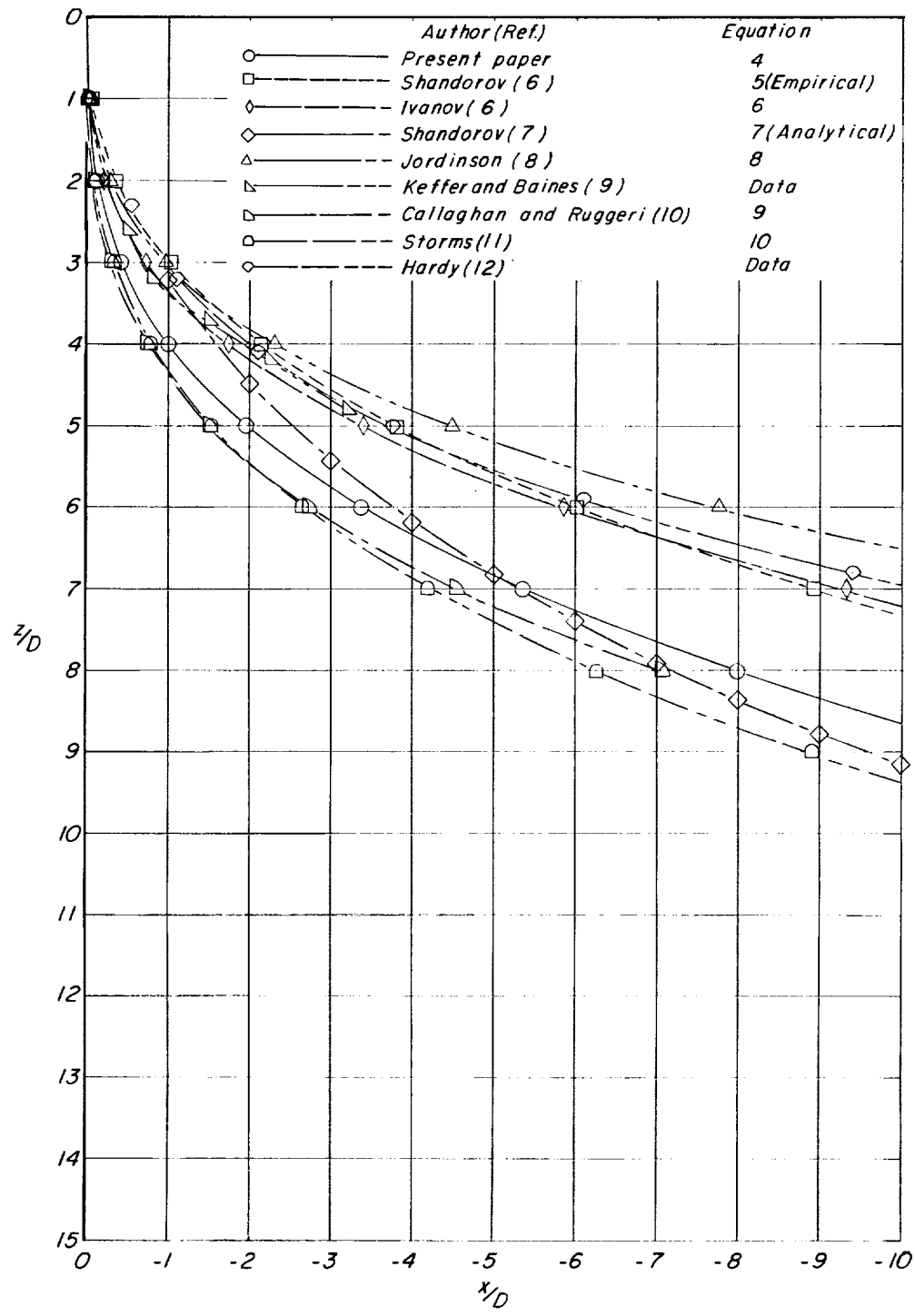

(d) V_e = 0.250.

Figure 18.- Continued.

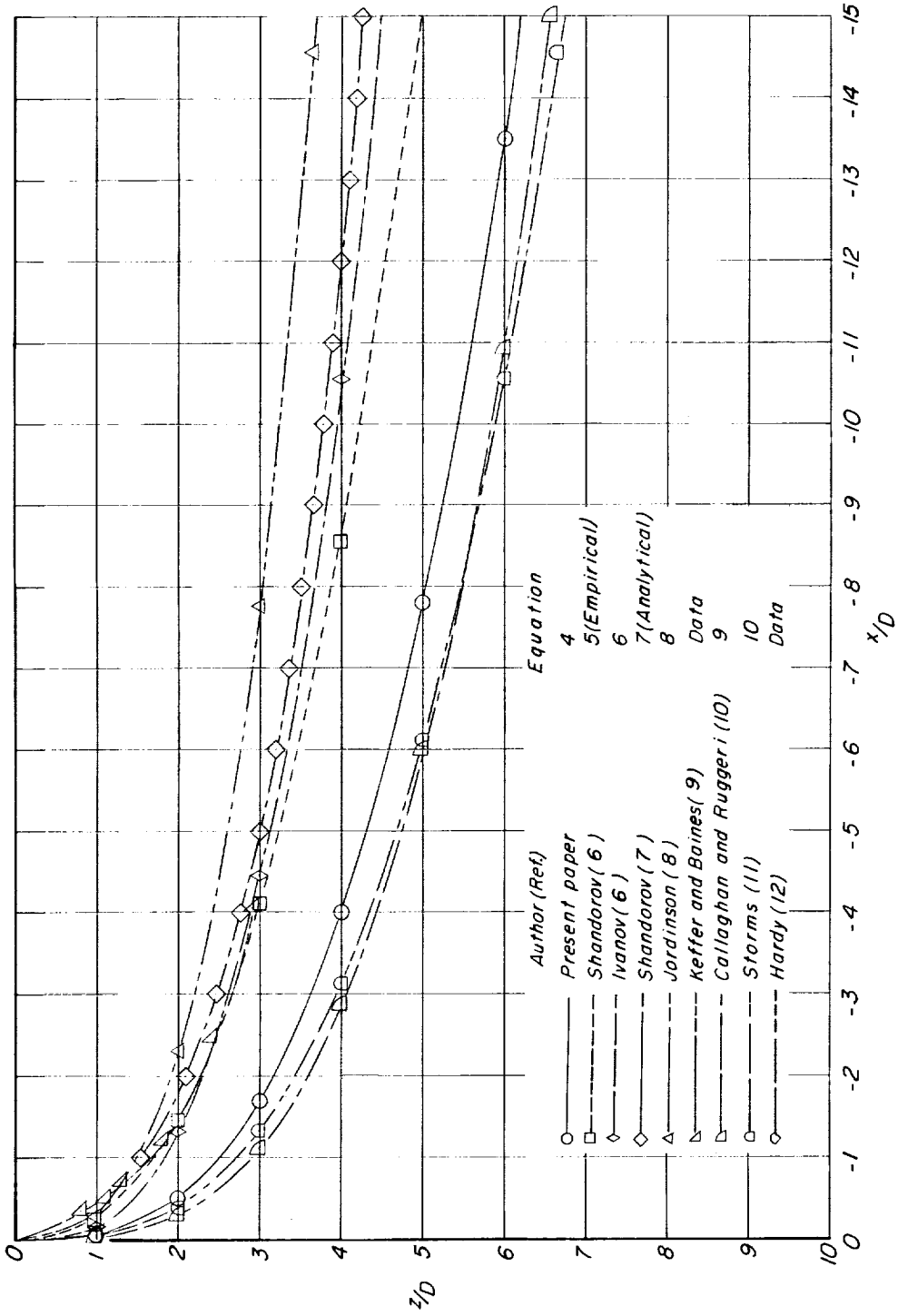

(e) $V_e = 0.500$.

Figure 18.- Concluded.

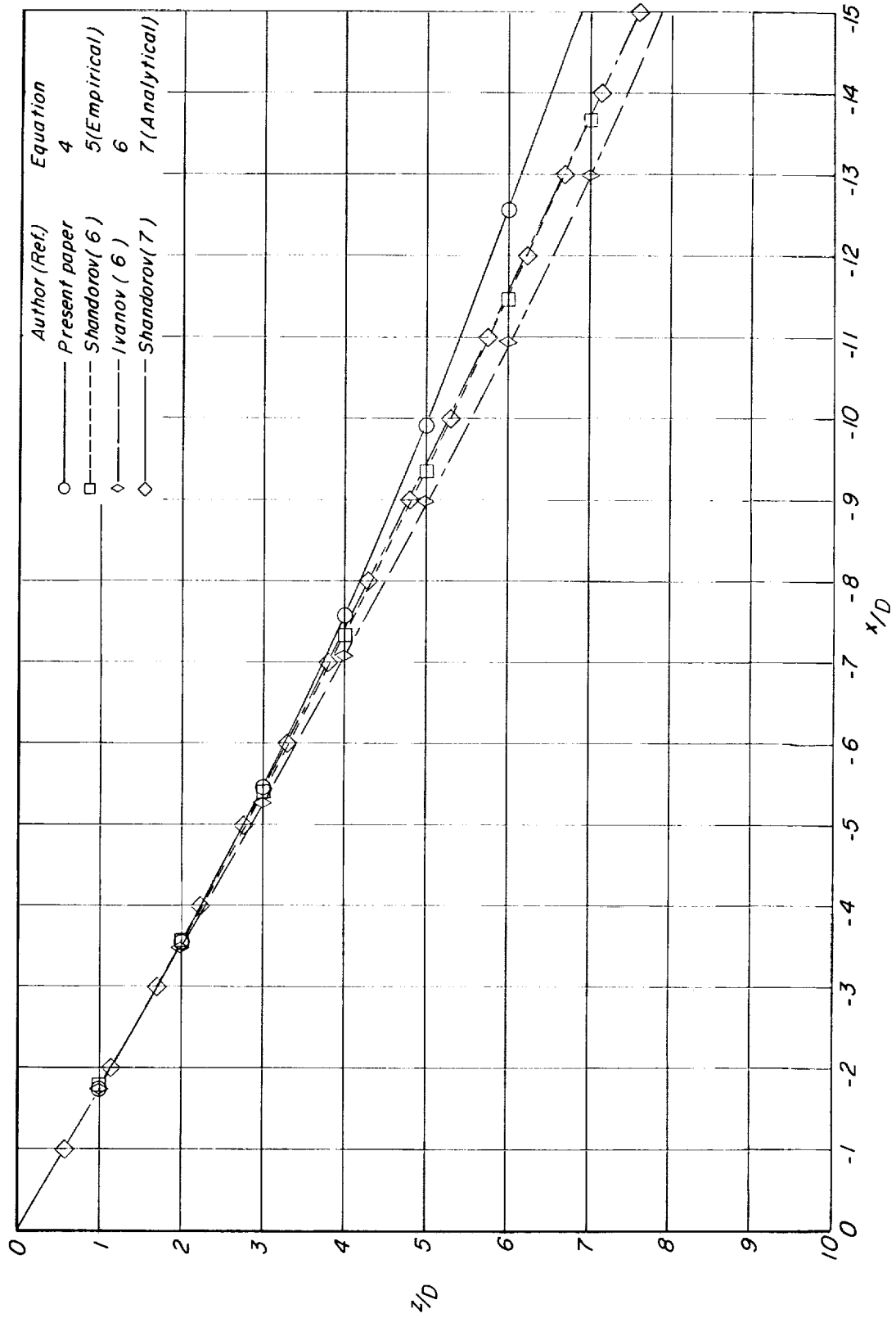

(a) $V_e = 0.100$.

Figure 19.- Comparison of jet wake path from equation (4) with results from references 6 and 7 at several effective velocity ratios. $\delta_j = 30^0$.

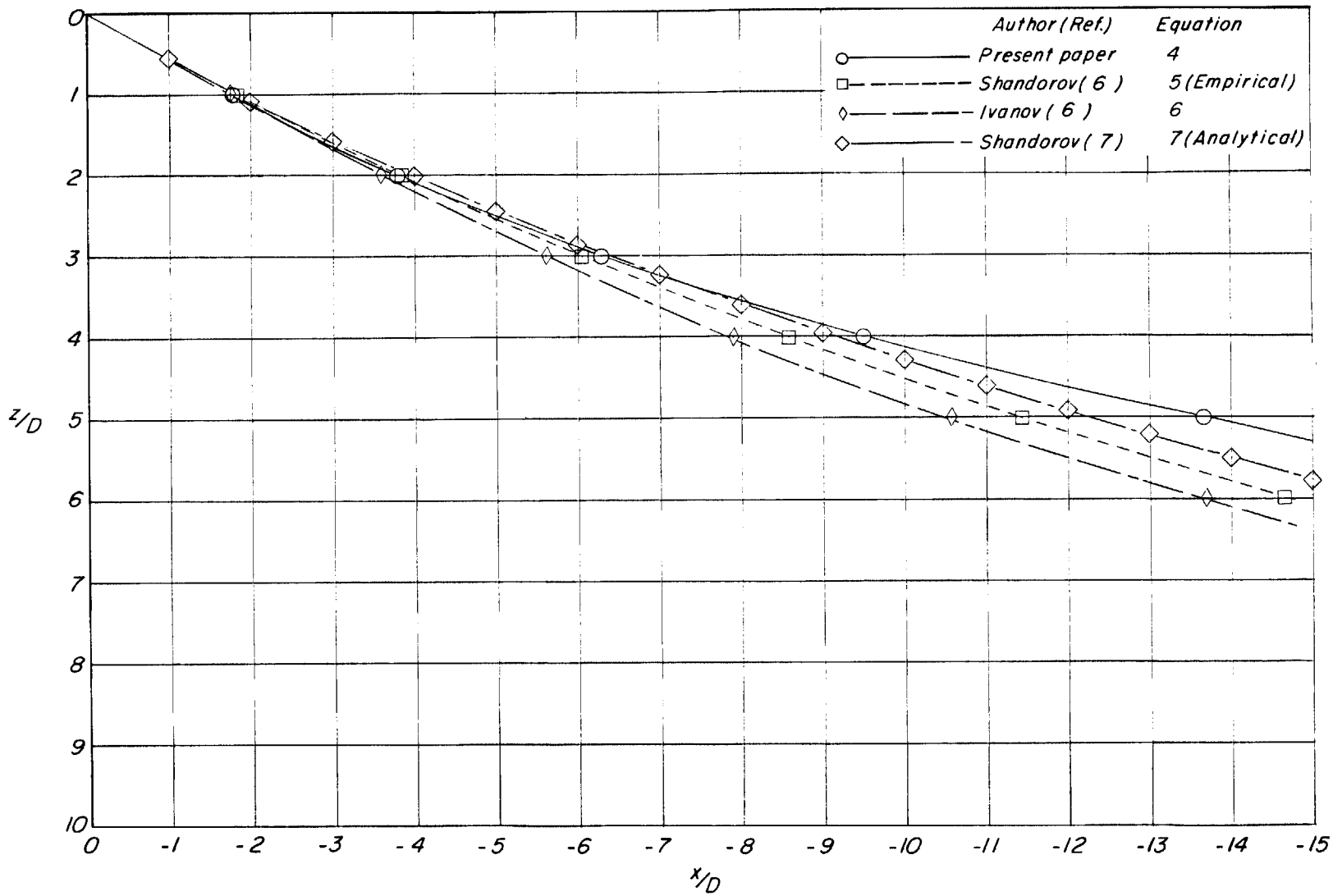

(b) $V_e = 0.200$.

Figure 19.- Continued.

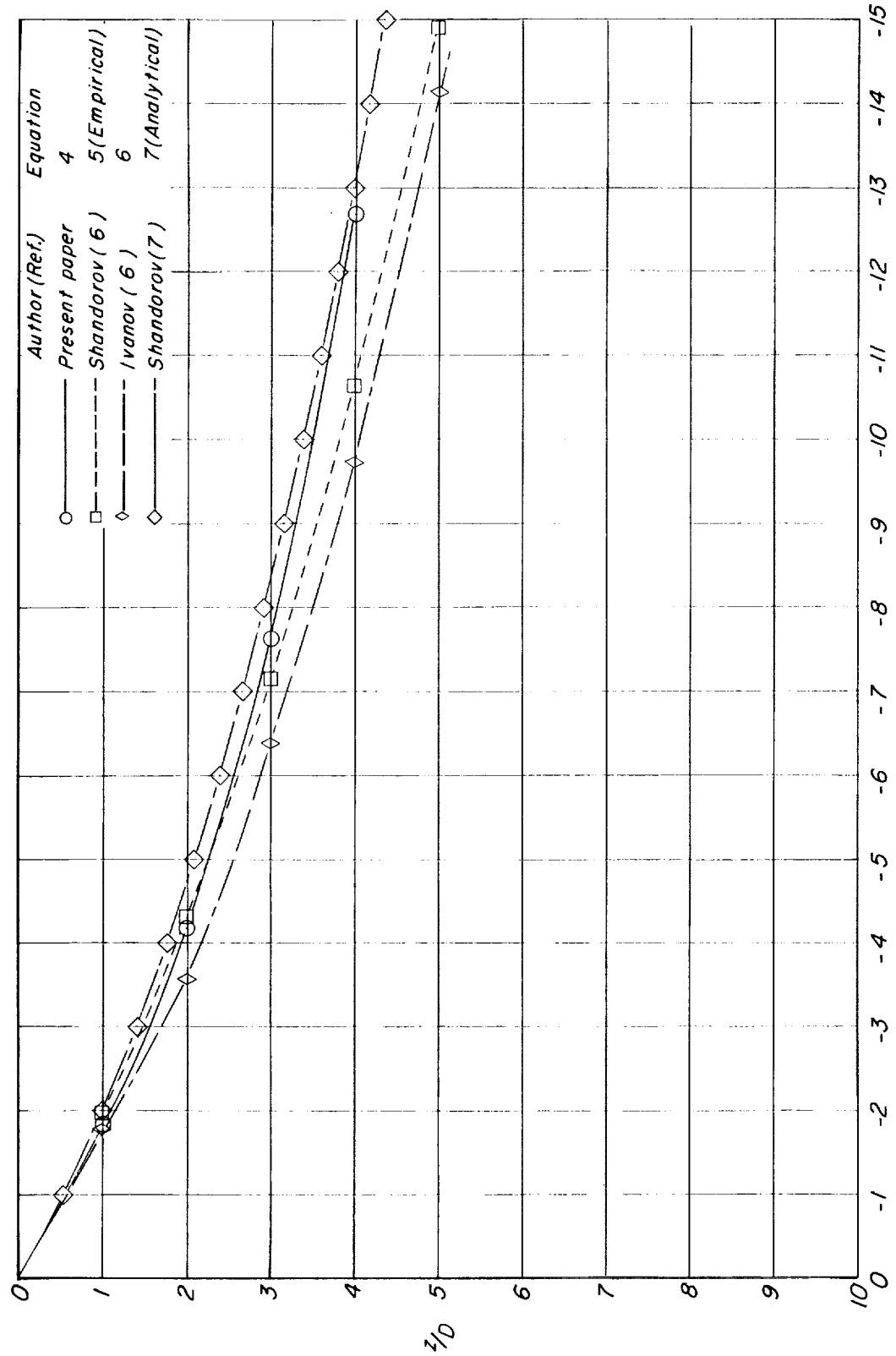

(c) $V_e = 0.300$.

Figure 19.- Concluded.

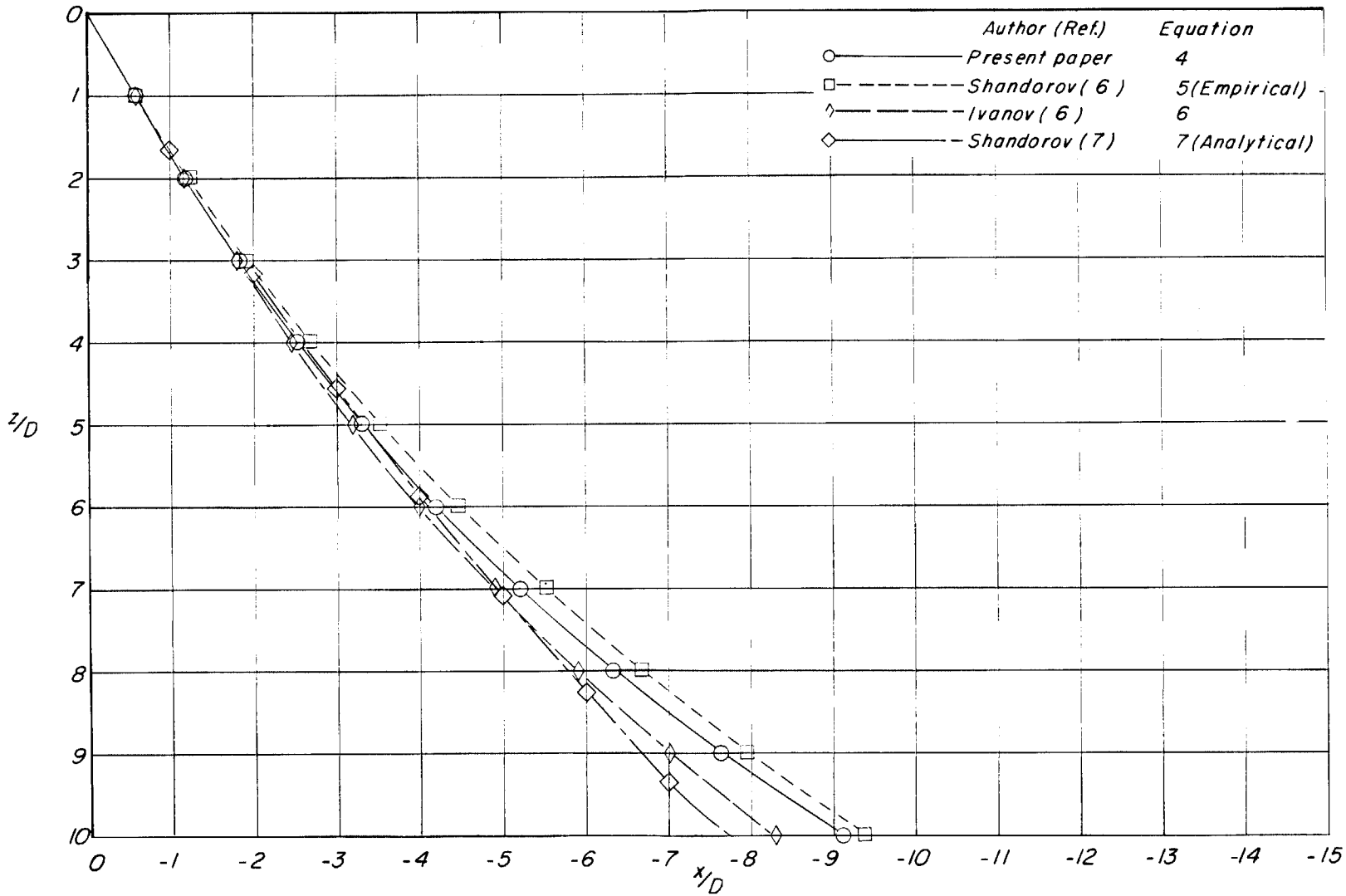

(a) $V_e = 0.100$.

Figure 20.- Comparison of jet wake path from equation (4) with results from references 6 and 7 at several effective velocity ratios. $\delta_j = 60^0$.

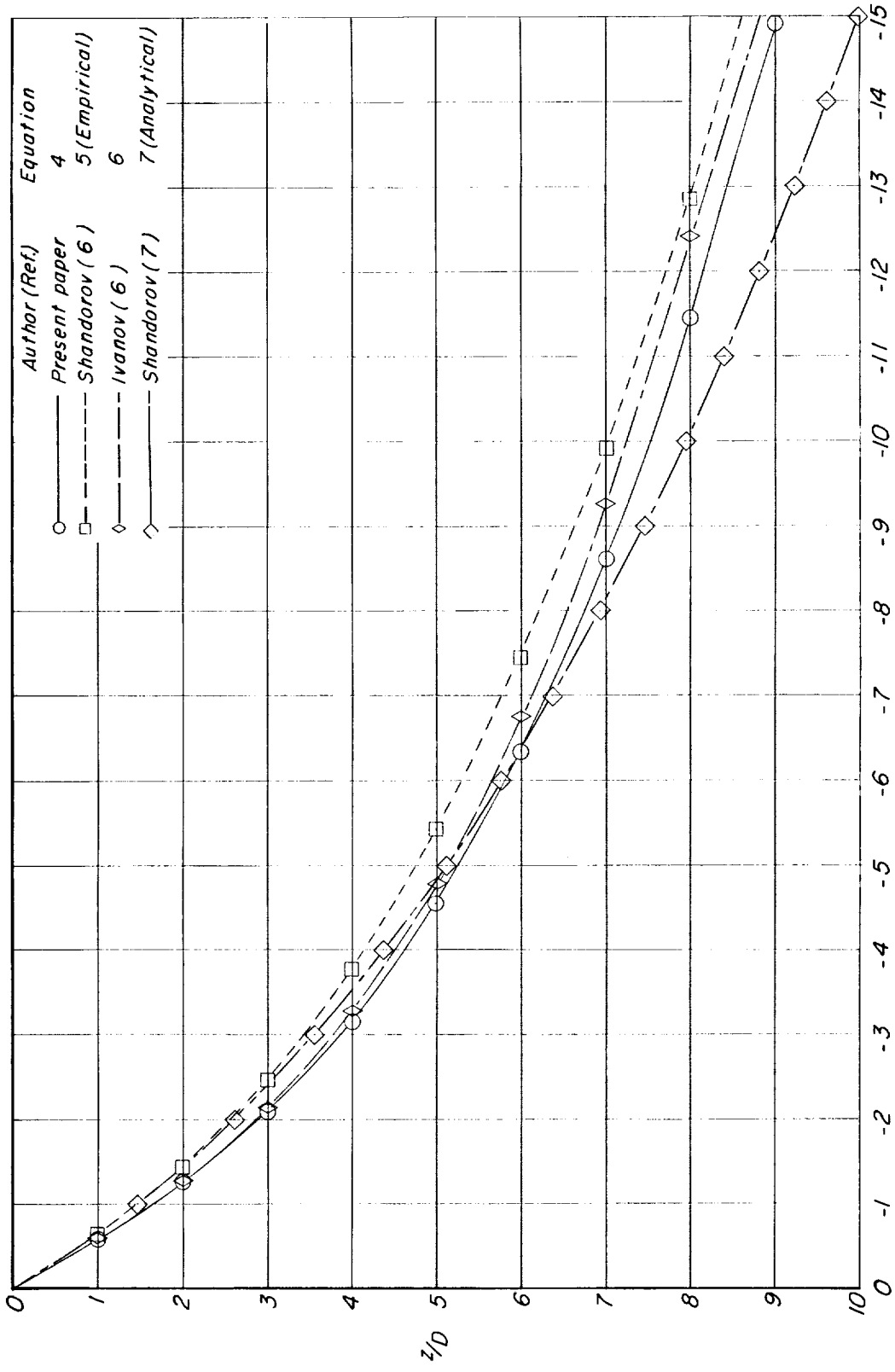

(b) $V_e = 0.200$.

Figure 20.- Continued.

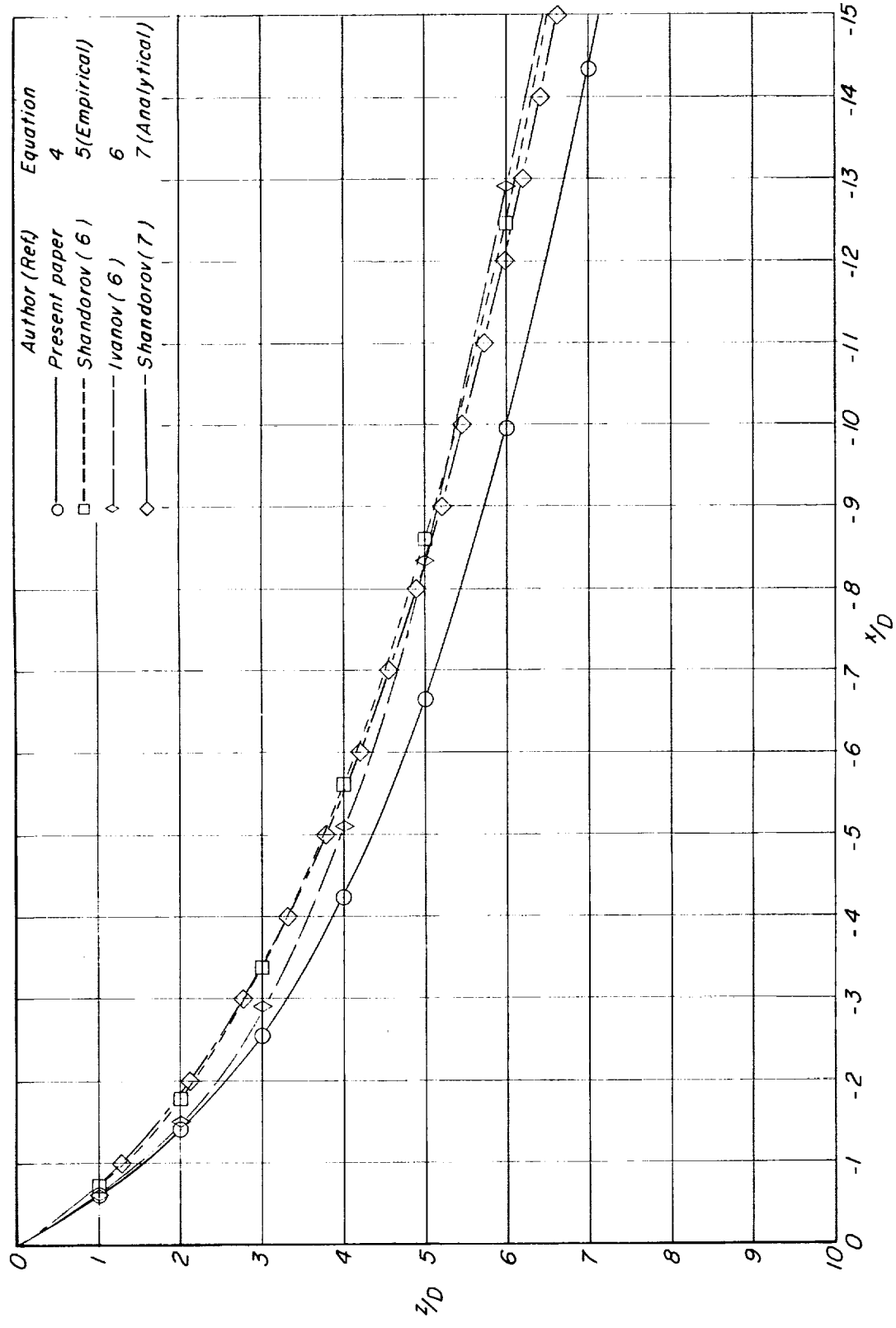

(c) $V_e = 0.300$.

Figure 20.- Concluded.

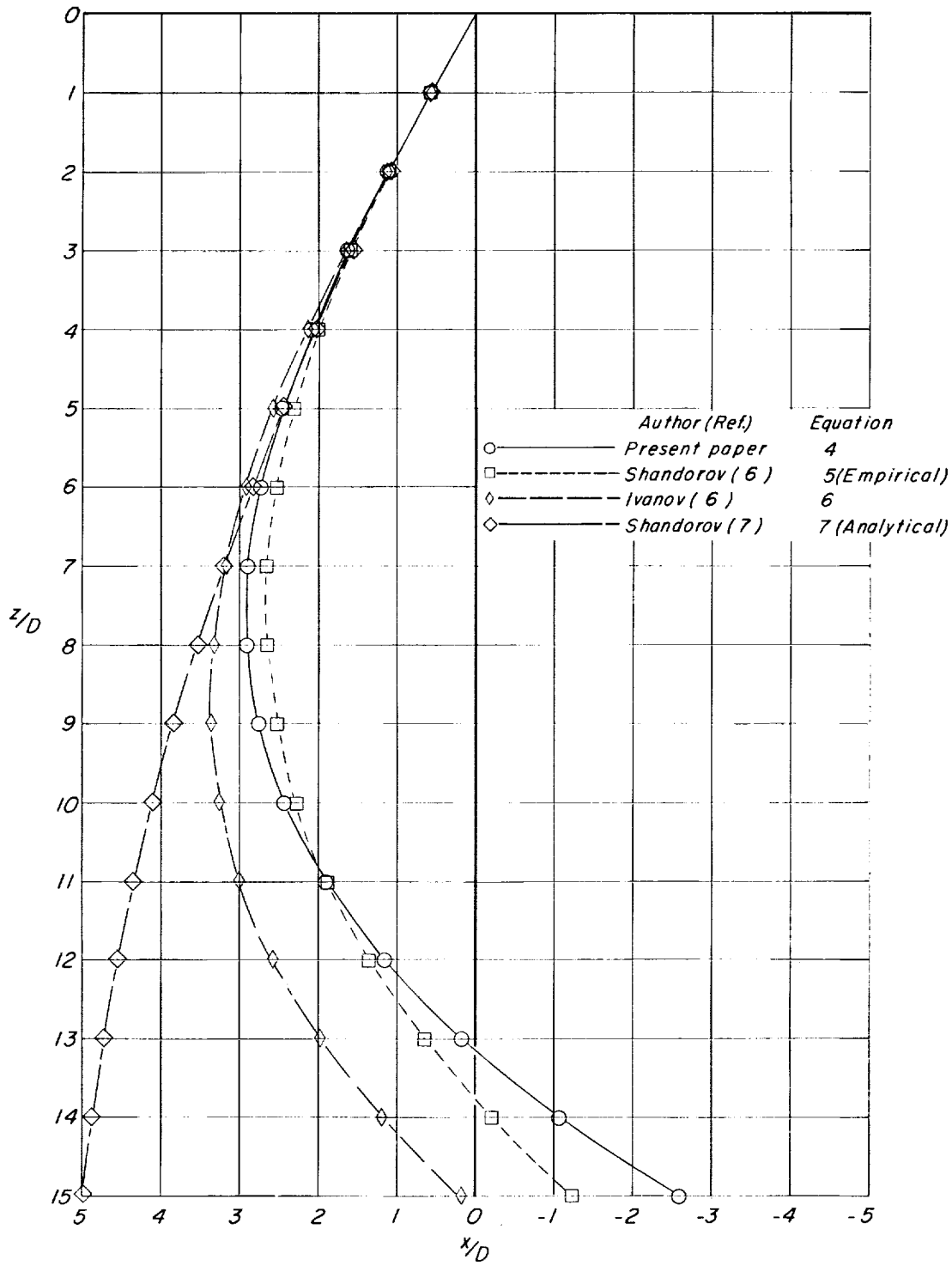

(a) $V_e = 120^0$.

Figure 21.- Comparison of jet wake path from equation (4) with results from references 6 and 7 at several effective velocity ratios. $\delta_j = 120^0$.

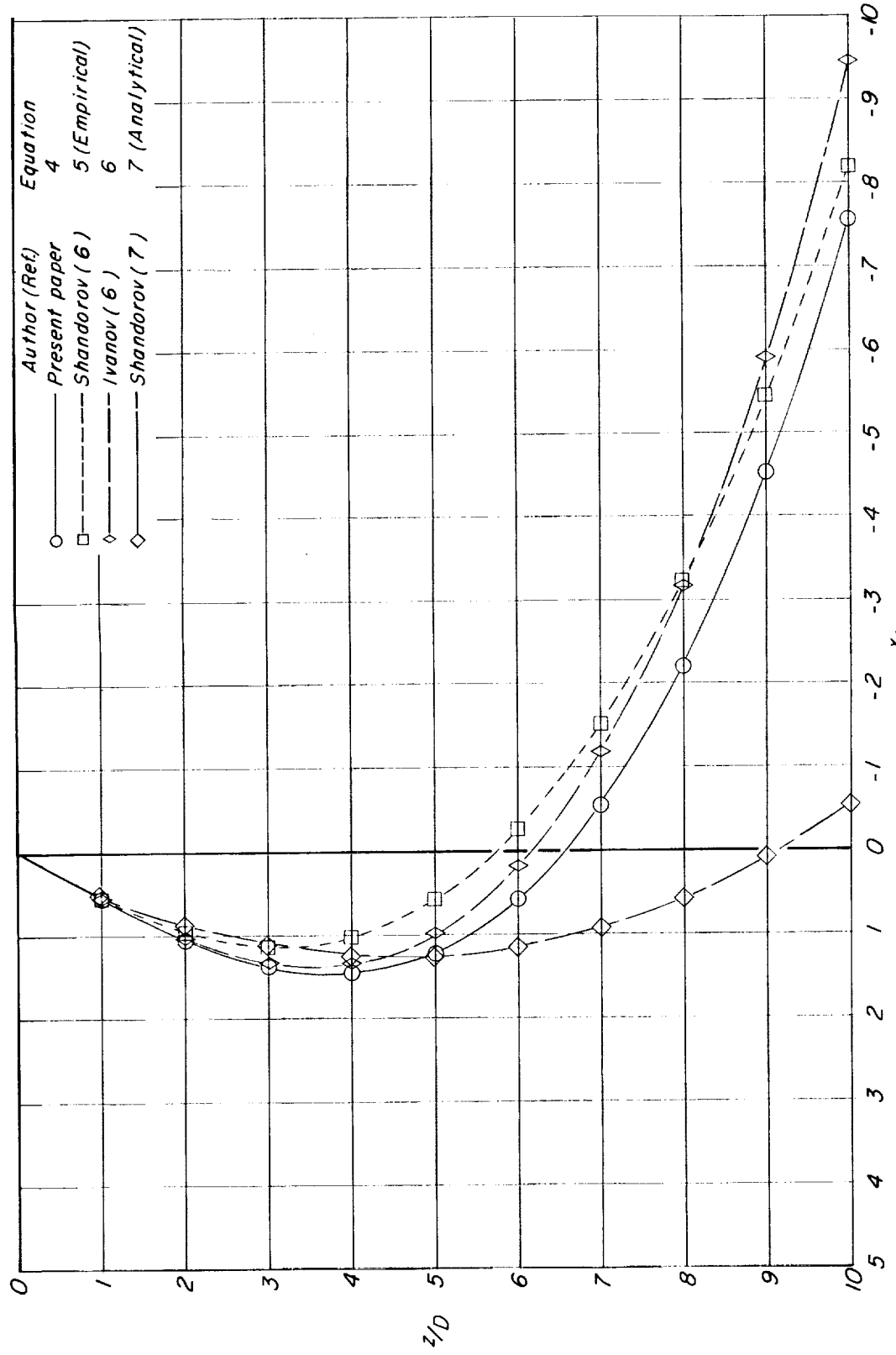

(b) $V_e = 0.200$.

Figure 21.- Continued.

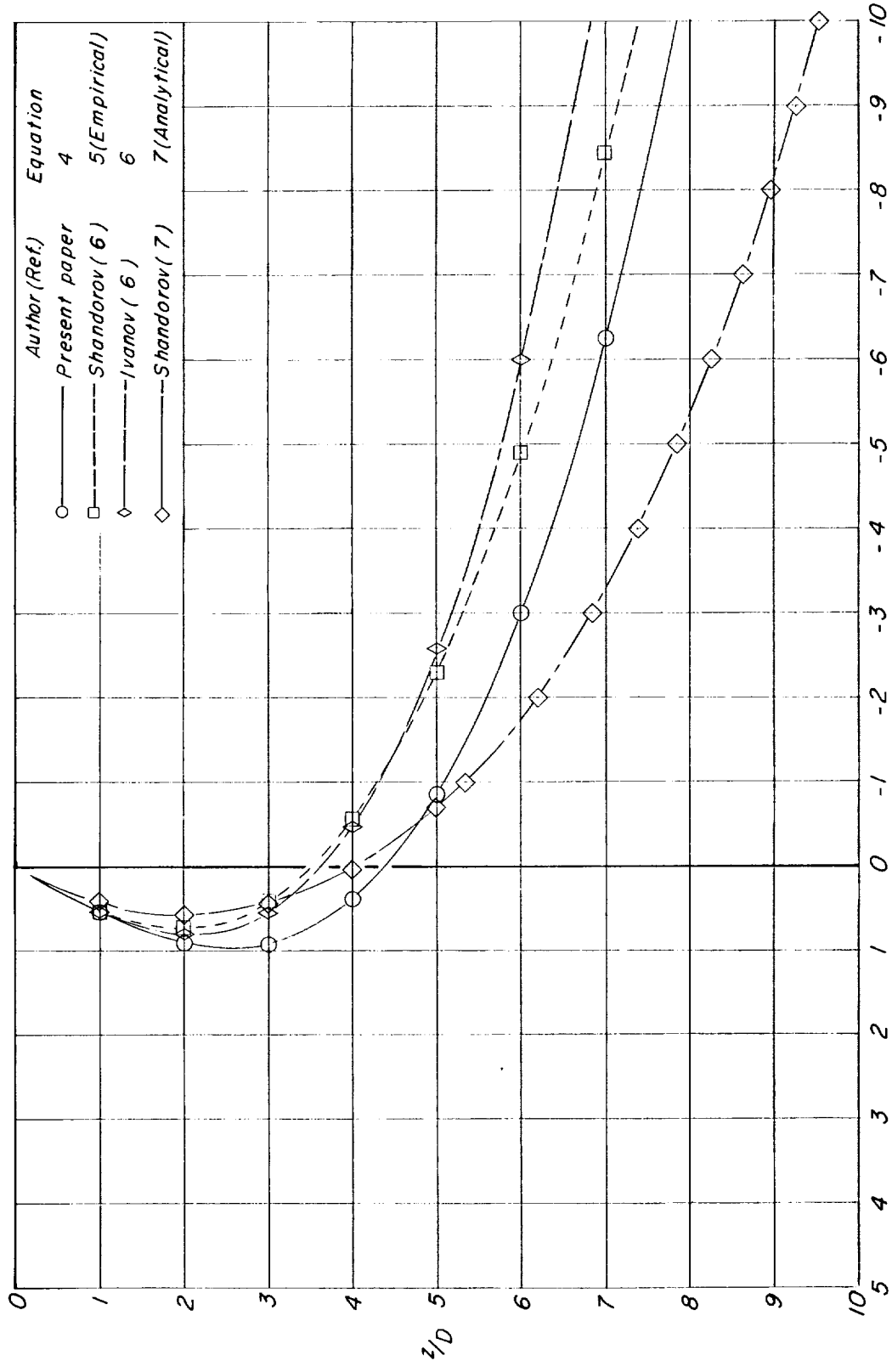

(c) $V_e = 0.300$.

Figure 21.- Continued.

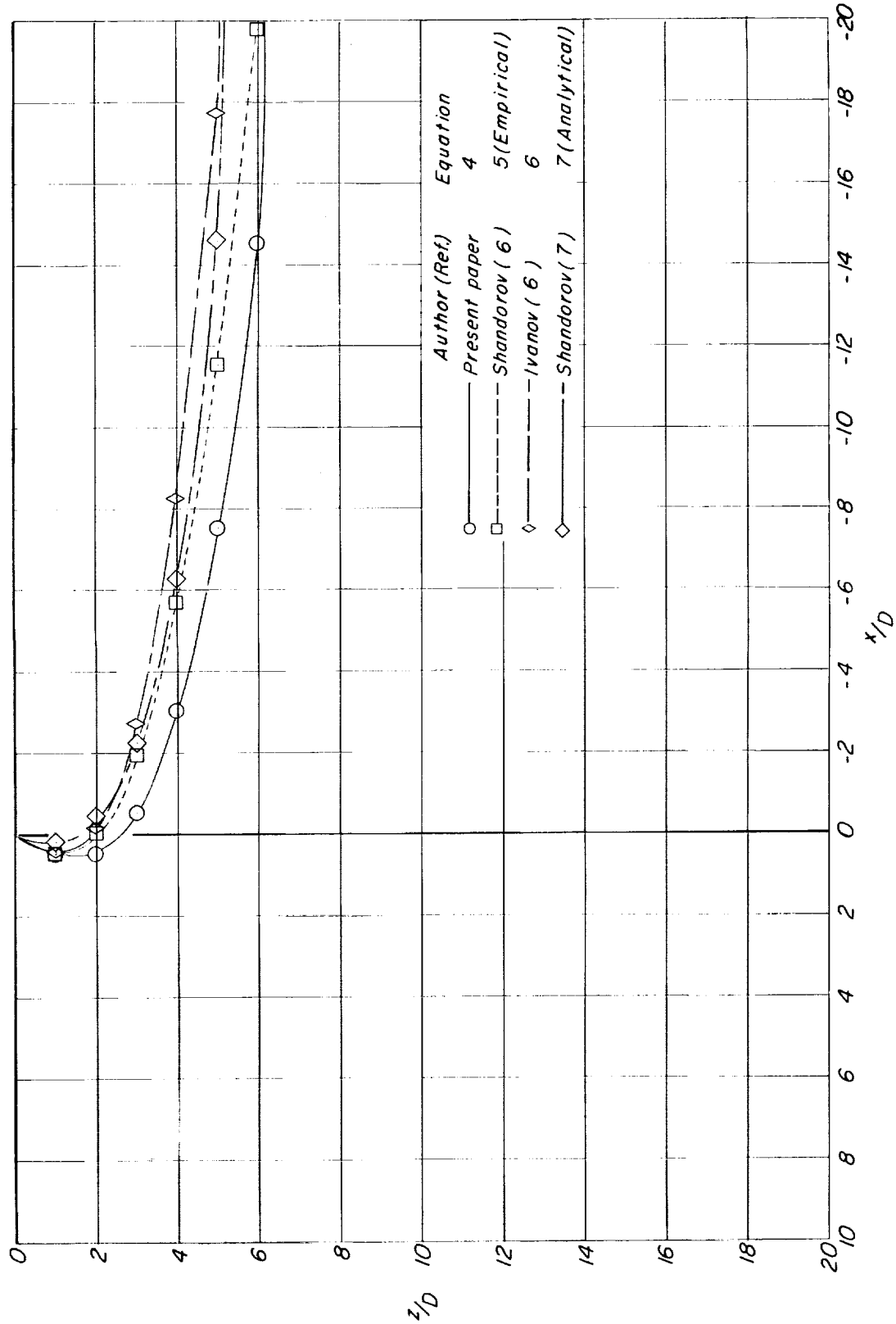

(d) $V_e = 0.500$.

Figure 21.- Concluded.

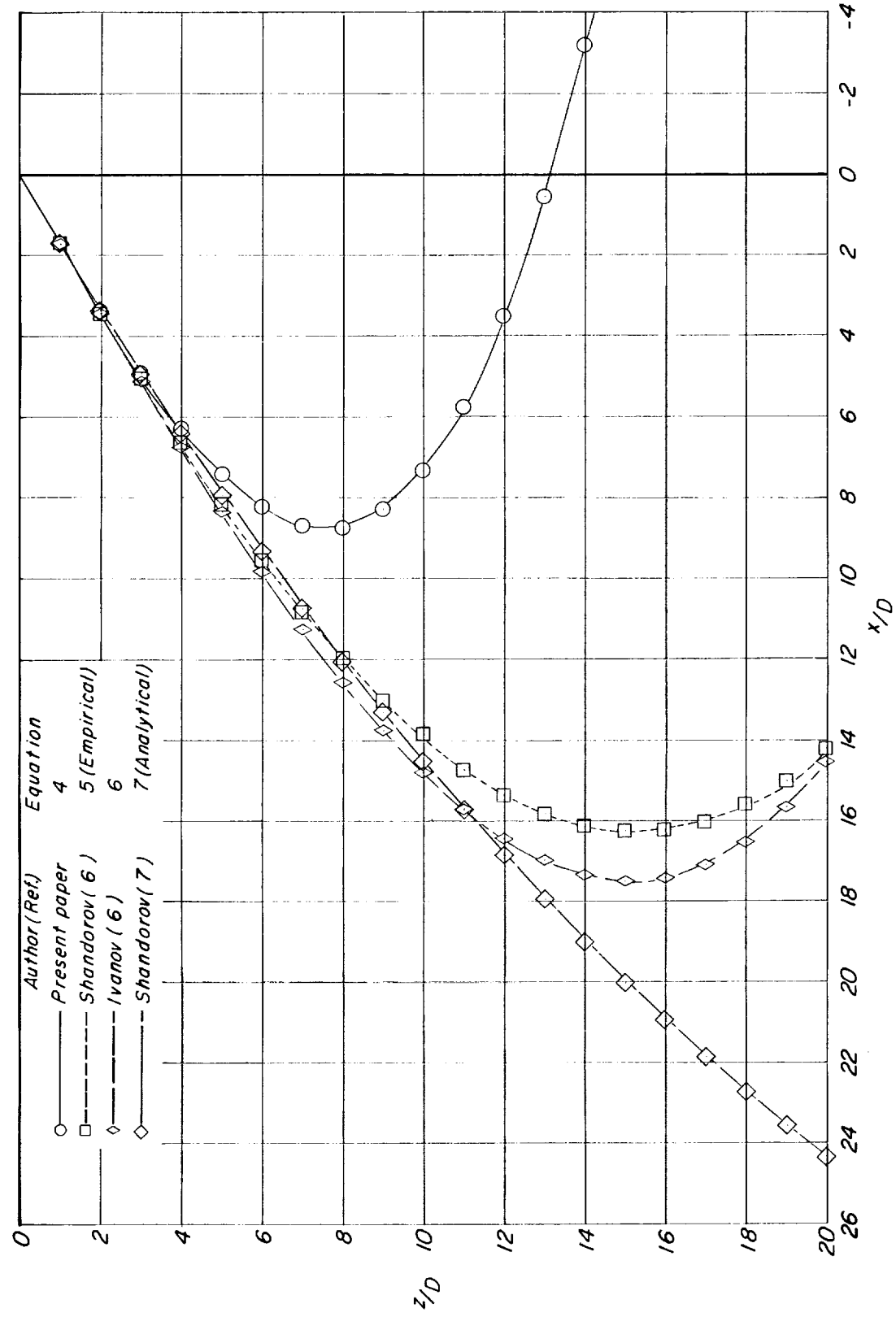

(a) $V_e = 0.100$.

Figure 22.- Comparison of jet wake path from equation (4) with results from references 6 and 7 at several effective velocity ratios. $\delta_j = 150^0$.

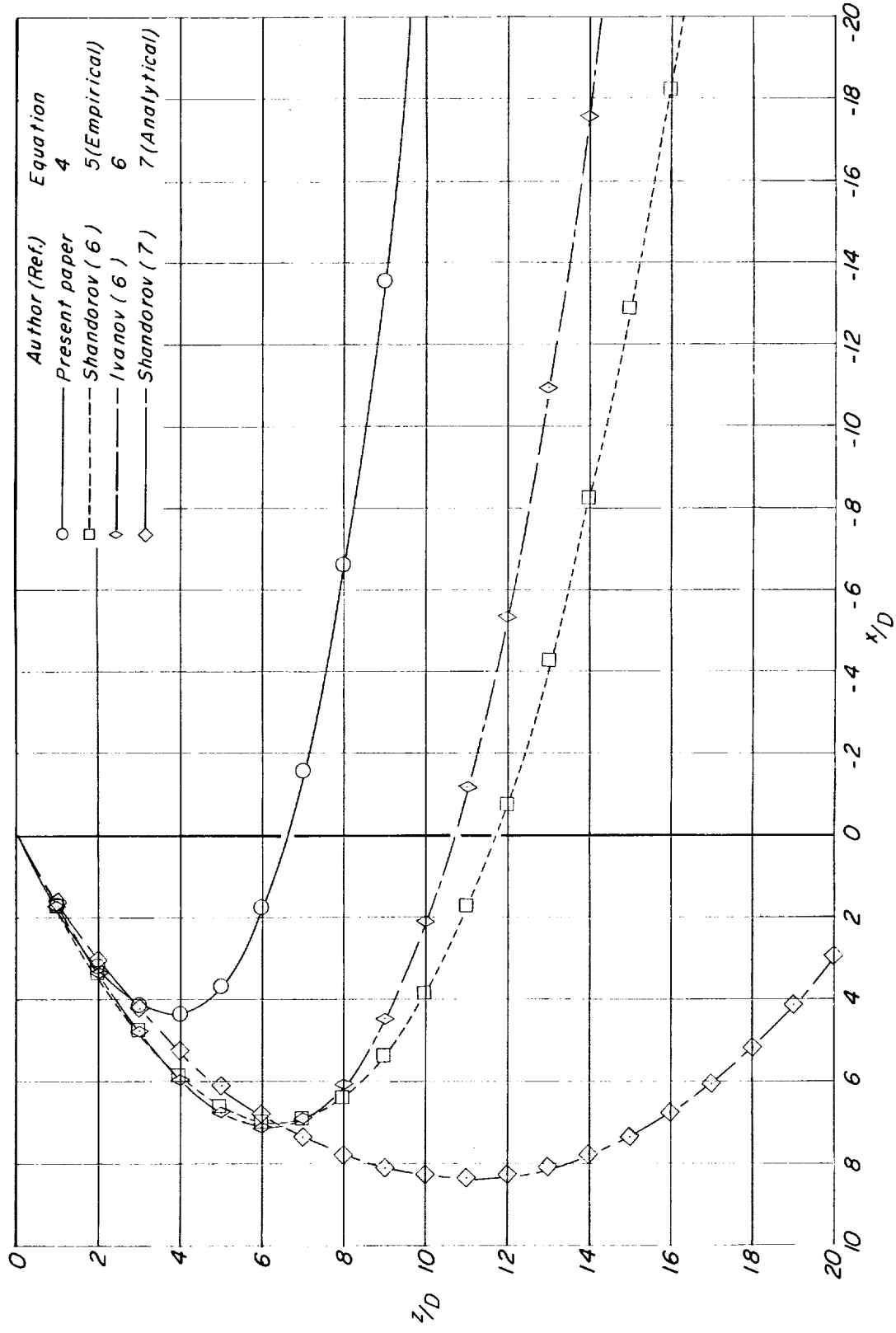

(b) $V_e = 0.200$.

Figure 22.- Continued.

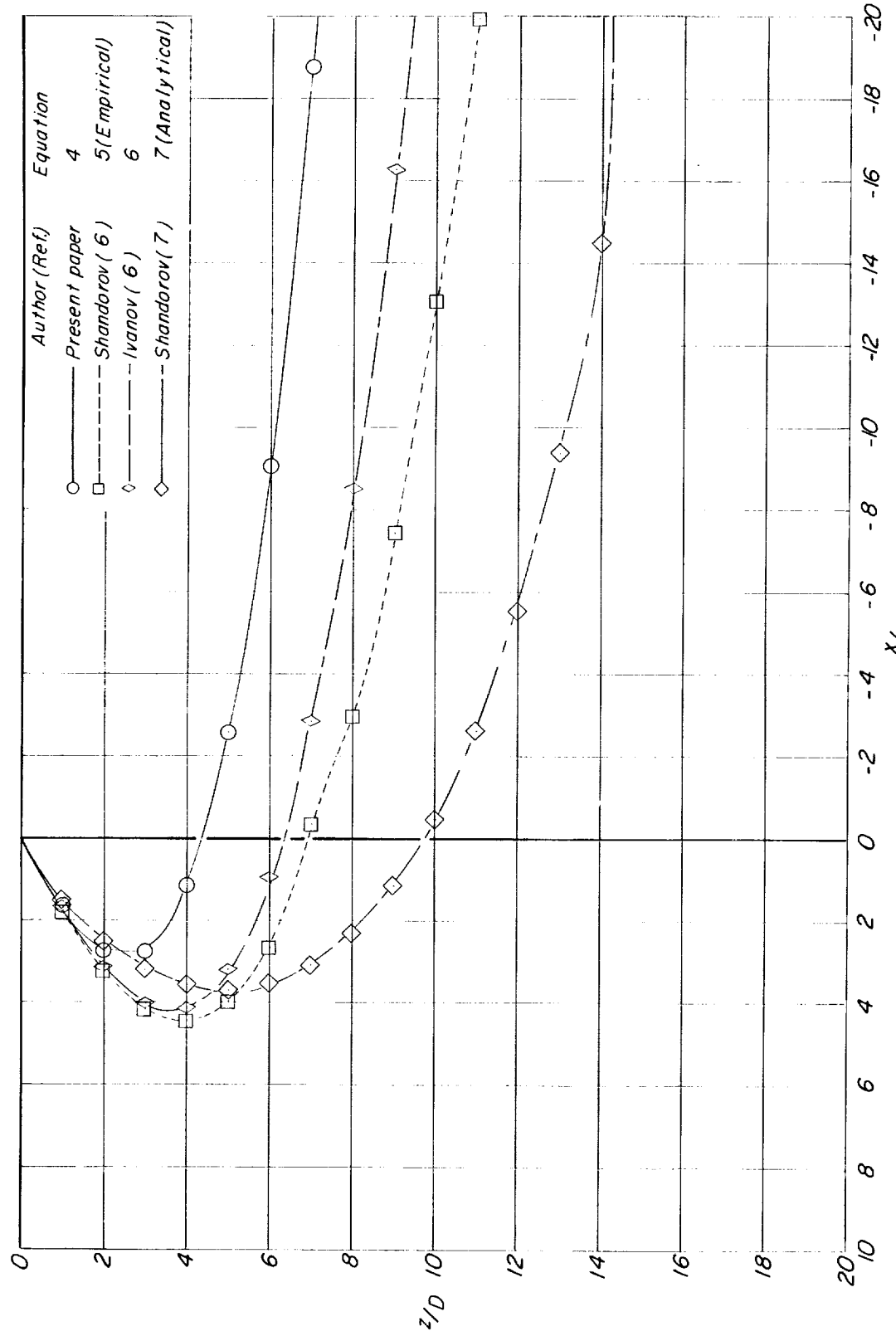

(c) $V_e = 0.300$.

Figure 22.- Continued.

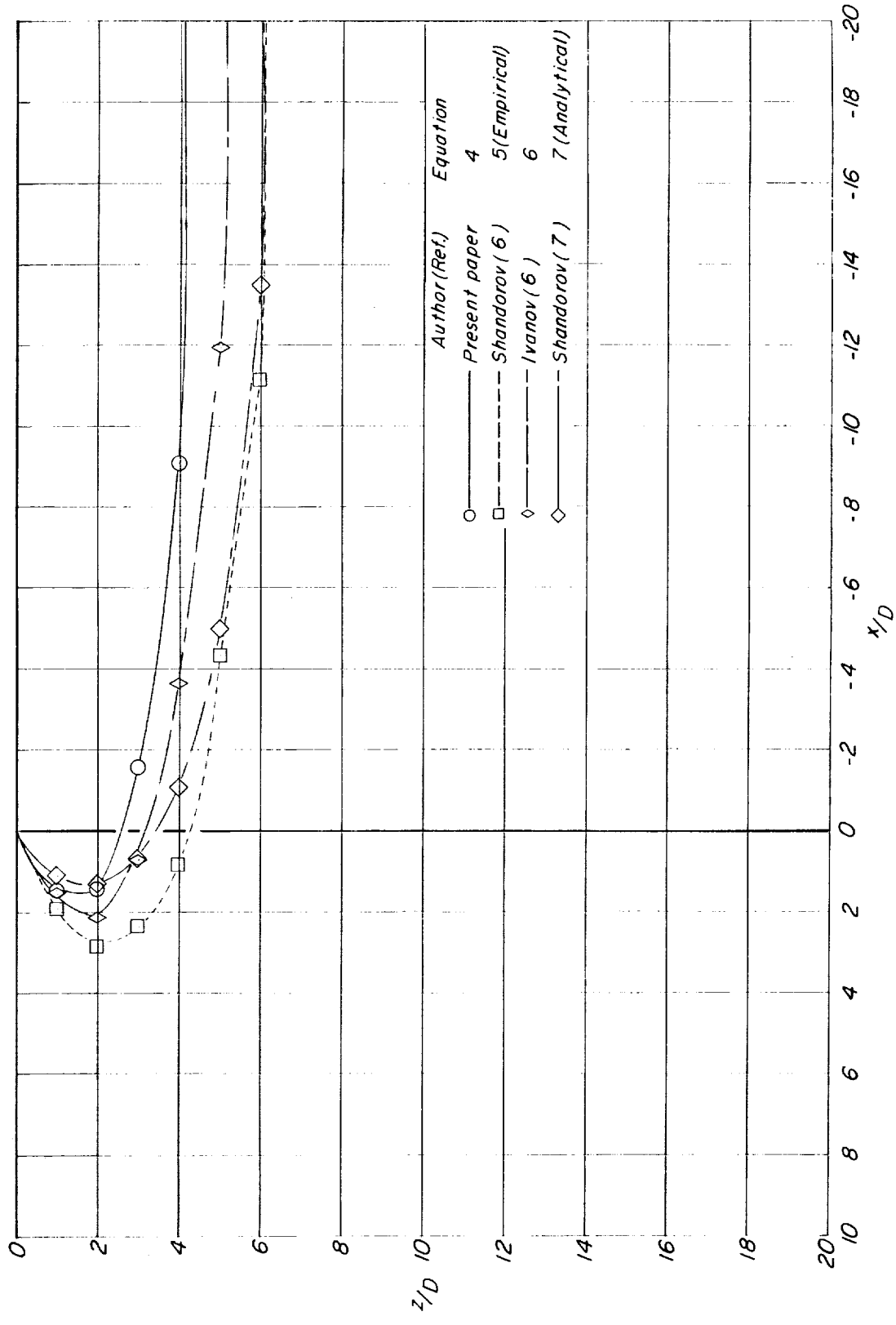

(d) $V_e = 0.500$.

Figure 22.- Concluded.

NASA-Langley, 1968 — 1 L-6144